

SUBSURFACE STRUCTURE OF THE CENTRAL THRACE BASIN FROM
3D SEISMIC REFLECTION DATA

A THESIS SUBMITTED TO
THE GRADUATE SCHOOL OF NATURAL AND APPLIED SCIENCES
OF
MIDDLE EAST TECHNICAL UNIVERSITY

BY

YERLAN TAIKULAKOV

IN PARTIAL FULFILLMENT OF THE REQUIREMENTS
FOR
THE DEGREE OF MASTER OF SCIENCE
IN
GEOLOGICAL ENGINEERING

JANUARY 2011

Approval of the thesis:

**SUBSURFACE STRUCTURE OF THE CENTRAL THRACE
BASIN FROM 3D SEISMIC REFLECTION DATA**

submitted by **YERLAN TAIKULAKOV** in partial fulfillment of the requirements for
the degree of **Master of Science in Geological Engineering Department, Middle East
Technical University** by,

Prof. Dr. Canan Özgen
Dean, Graduate School of **Natural and Applied Sciences**

Prof. Dr. Zeki Çamur
Head of Department, **Geological Engineering**

Assist. Prof. Dr. A. Arda Özacar
Supervisor, **Geological Engineering Dept., METU**

Assoc. Prof. Dr. Nuretdin Kaymakçı
Co-Supervisor, **Geological Engineering Dept., METU**

Examining Committee Members:

Prof. Dr. Erdin Bozkurt
Head of Jury, Geological Engineering Dept., METU

Assist. Prof. Dr. A. Arda Özacar
Supervisor, Geological Engineering Dept., METU

Assoc. Prof. Dr. Nuretdin Kaymakçı
Co-Supervisor, Geological Engineering Dept., METU

Dr. Özgür Sipahioğlu
Turkish Petroleum Corporation

M.Sc. Cenk Yardımcılar
Cenk-Abdukadir Petrol Danışmanlık

Date: 7.01.2011

I hereby declare that all information in this document has been obtained and presented in accordance with academic rules and ethical conduct. I also declare that, as required by these rules and conduct, I have fully cited and referenced all material and results that are not original to this work.

Name, Last name: YERLAN TAIKULAKOV

Signature:

ABSTRACT

SUBSURFACE STRUCTURE OF THE CENTRAL THRACE BASIN FROM 3D SEISMIC REFLECTION DATA

Yerlan, Taikulakov

M.Sc., Department of Geological Engineering

Supervisor: Assist. Prof. Dr. A. Arda Özacar

Co-Supervisor: Assoc. Prof. Dr. Nuretdin Kaymakçı

January 2011, 68 pages

The Thrace Basin located in northwest Turkey displays attractive prospective traps for hydrocarbon and has received much attention from the petroleum industry. Despite the extensive exploration efforts, there are only few studies which address the fault kinematics and deformation mechanism of the region in connection with structural development. In this study, 3D raw seismic data set collected around Temrez High near Babaeski fault zone will be processed and interpreted along with the available borehole data to reveal the subsurface structure of the region that will contribute towards understanding the Neogene tectonic evolution of the central Thrace basin, origin of the transcurrent tectonics and possible role of the North Anatolian Fault Zone.

Keywords: Thrace Basin, Fault Zone, Evolution, Processing, Stratigraphy.

ÖZ

ORTA TRAKYA HAVZASININ YERALTI YAPISININ ÜÇ BOYUTLU SİSMİK YANSIMA VERİSİ İLE ANALİZİ

Yerlan, Taikulakov

Yüksek Lisans, Jeoloji Mühendisliği Bölümü

Tez Yöneticisi: Doç. Dr. A. Arda Özacar

Ortak Tez Yöneticisi: Yrd. Doç. Dr. Nuretdin Kaymakçı

Ocak 2011, 68 sayfa

Kuzeybatı Türkiye de yer alan Trakya havzası etkileyici hidrokarbon kapanları barındırmaktadır ve bu nedenle petrol endüstrisinin ilgisini çekmektedir. Yoğun arama çabalarına karşın, sadece bir kaç çalışma, bölgedeki fay kinematiği ve deformasyon mekanizmasını yapısal havza gelişimi ile ilişkilendirerek incelemiştir. Bu çalışmada, Babaeski fay zonu yakınındaki Temrez yükseliminden toplanmış üç boyutlu işlenmemiş sismik veri seti işlenmiş ve kuyu ölçümleri ile yorumlanmıştır. Bölgenin yeraltı yapısını ortaya koyan sonuçlar, orta Trakya havzasının Neojen tektonik evriminin, etkin yanal atımlı tektonizmanın kökeninin ve bölgede Kuzey Anadolu Fay Zonunun olası rolünün anlaşılmasına katkı koyacaktır.

Anahtar kelimeler: Trakya havzası, Fay zonu, Gelişim, İşleme, Stratigrafi.

To my Dear Father

ACKNOWLEDGEMENTS

I would like to thank my supervisor Assist. Prof. Dr. A. Arda Özacar, who has persistently navigated me and supported with valuable advices until the end of M.Sc. Thesis.

I am deeply grateful to my co-supervisor Assoc. Prof. Dr. Nuredtin Kaymakçı for the further development of my M.Sc. research.

I owe my deepest gratitude to the crew of CAPD Company, especially to Cenk Yardımcılar, Abdukadir Yılmaz and Ali Meral for 3D seismic data set, invaluable support, persistent encouragement and remarkable advice throughout my M.Sc. studies. In addition, I want to thank for the licenses of the Paradigm Focus and STM Kingdom Suit software that were provided for this studies. These people deserve most respect and appreciation.

Furthermore, I acknowledge the committee of the thesis, Prof. Dr. Erdin Bozkurt and Dr. Özgür Sipahioğlu for their thoughtful comments and suggestions.

Finally, I would like to express deepest appreciation to my family, especially to Taikulakov Yengelsbek Taltusovich and Taikulakova Gulnara Serikovna.

TABLE OF CONTENTS

ABSTRACT	iv
ÖZ	v
ACKNOWLEDGEMENTS.....	vii
TABLE OF CONTENTS.....	viii
LIST OF FIGURES	x

CHAPTERS:

1. INTRODUCTION.....	1
1.1 PURPOSE AND SCOPE.....	1
1.2 STUDY AREA.....	2
1.3 DATA AND METHOD OF STUDY	3
1.3.1 3D Seismic Data Acquisition	3
1.3.2 Borehole Data.....	4
1.3.3 Seismic Processing and Interpretation	5
1.4 PREVIOUS STUDIES	6
2. GEOLOGY	10
2.1 REGIONAL STRATIGRAPHY.....	10
2.2 REGIONAL TECTONIC STRUCTURES.....	15
2.3 GEOLOGICAL EVOLUTION	17
2.4 LOCAL STRATIGRAPHY	18
2.5 LOCAL TECTONIC STRUCTURES	23
3. SEISMIC DATA PROCESSING	25
3.1 DATA PREPARATION	26
3.2 FREQUENCY FILTERING.....	27
3.3 GAIN CORRECTION	27
3.4 DECONVOLUTION	29
3.5 GATHER	30

3.6	STATIC CORRECTION	31
3.7	VELOCITY ANALYSIS.....	32
3.8	DIP MOVE-OUT (DMO) CORRECTION	35
3.9	MIGRATION.....	38
4.	SEISMIC INTERPRETATION	43
4.1	WELL-TO-SEISMIC TYING AND HORIZON PICKING	43
4.2	FOLDS	48
4.3	FAULT INTERPRETATION	49
5.	DISCUSSION AND CONCLUSIONS	60
	REFERENCES.....	64

LIST OF FIGURES

FIGURES:

Figure 1: Location map of the study area. Satellite image is taken from Google Earth.	2
Figure 2: Fold map of the Temrez 3D survey.	3
Figure 3: Map of the Temrez 3D seismic survey showing the location of wells (red circles) used in this study along with their maximum depths.	4
Figure 4: Schematic representation of data acquisition, initial and processed data in seismic reflection method.	5
Figure 5: Geology map of the Thrace Basin taken from Siyako, et al. (2007).	12
Figure 6: Generalized lithostratigraphic section of the Thrace Basin taken from S��nnet��io��lu (2008).	13
Figure 7: Generalized chronostratigraphic chart of the Thrace Basin taken from S��nnet��io��lu (2008). Numbers at the top of the figure correspond to the locations shown in the inset map.	14
Figure 8: The geological cross-section depicting major structures of the Thrace Basin. Location of the section is indicated in the inset map. TFS, Thrace Fault System; GF, Ganos Fault; (G��r��r, et al., 1996).	15
Figure 9: Structural map of the northwest Turkey (Yaltırak 2002, Kaymak��ı et al. 2007). TEFZ: Thrace-Eski��ehir Fault Zone, KFZ: Kırklareli Fault Zone, LFZ: L��leburgaz Fault Zone, BFZ: Babaeski Fault Zone, NAFNS: Northern Strand, NAFMS: Middle Strand, NAFSS: Southern Strand of the North Anatolian Fault.	16

Figure 10: The stratigraphic columnar section of the study area after Turgut et al. (2000). Note that thickness information are derived from available borehole data.	18
Figure 11: a) Well log correlation along transects running between boreholes used in the study area. b) Map showing the location of the section. TD, Total depth;.....	22
Figure 12: The map showing the geology, structural settings and location of the study area (redrawn from Perinçek 1991).	23
Figure 13: The interpreted 2D seismic section showing the positive flower structure along the Babaeski Fault Zone (taken from Perinçek, 1991). Location of the seismic section is shown in Figure 12.	24
Figure 14: Seismic data re-processing sequence used in this study.	25
Figure 15: Quality Control of the 3D seismic data geometry.	26
Figure 16: a) Raw shot gathers. b) Shot gathers after trace editing, surface consistent amplitude balancing and frequency filtering. c) Shot gathers after gain correction.	28
Figure 17: Shot gathers after deconvolution.	30
Figure 18: Simple illustrated example of common mid-point (CMP) gathering taken from Lillie (1999).	30
Figure 19: a) Datum statics terminology. b) Floating datum statics of the study area.	31
Figure 20: Results of the velocity analysis and normal moveout (NMO) correction (velocity spectrum, shot gather and stacks) conducted using updated residual statics. Note that the picked NMO corrected stacking velocity function (4) is shown in bold.	33
Figure 21: Seismic cross-section (crossline no: 2262) of stacked data after normal moveout (NMO) correction. Location of the cross section is shown in inset map along with boreholes.	34

Figure 22: Results of the velocity analysis and dip moveout (DMO) correction (velocity spectrum, shot gather and stacks) conducted using final datum statics. Note that the picked DMO corrected stacking velocity function (4) is shown in bold.....	36
Figure 23: Seismic cross-section (crossline no: 2262) of stacked data after dip moveout (DMO) correction. Location of the cross section is shown in inset map along with boreholes.	37
Figure 24: Results of the migration velocity analysis (velocity spectrum, shot gather and stacks) conducted Note that the picked migration velocity function (4) is shown in bold.	39
Figure 25: Seismic cross-section (crossline no: 2262) of stacked data after pre-stack time migration. Location of the cross section is shown in inset map along with boreholes.	40
Figure 26: Interval velocity model of the seismic cross-section (crossline no: 2262). Location of the cross section is shown in inset map along with boreholes.	40
Figure 27: Seismic cross-sections (inline no: 5257). a) Before re-processing; b) after re-processing. Location of the cross section is shown in inset map along with boreholes.	41
Figure 28: Seismic timeslices at 0.5 sec. a) Before re-processing; b) after re-processing.....	42
Figure 29: a) Seismic cross-section passing along the two boreholes located within the study area. b) Map of the study area showing the location of the cross-section, boreholes and 2D seismic line (no: DD-1388) used to tie the Kozpınar-1 well. KP-1: Kozpınar-1, PK-1: Pancarköy-1, KK-1: Karakavak-1.	44
Figure 30: Seismic sections showing the unconformity surface at the top of the Danişmen formation.....	45
Figure 31: Color coded contour maps of the picked horizon tops of the formations in time domain.	47

Figure 32: Color-coded isochron maps of a) Osmancık b) Mezardere formations and c) Ceylan group.	48
Figure 33: Doubly plunging anticlines observed in the study area. a) time slices at 1 sec, b) color coded time contour map of the top of Osmancık Formation. BA: Babaeski Anticline, KKA: Karakavak Anticline.	49
Figure 34: Raw and interpreted seismic cross-sections in time. Location of the cross-section is shown in the inset map along with boreholes and recognized faults.	50
Figure 35: Raw and interpreted seismic cross-sections in time. Location of the cross-section is shown in the inset map along with boreholes and recognized faults.	51
Figure 36: Raw and interpreted seismic cross-sections in time. Location of the cross-section is shown in the inset map along with boreholes and recognized faults.	52
Figure 37: Raw and interpreted seismic cross-sections in time. Location of the cross-section is shown in the inset map along with boreholes and recognized faults.	53
Figure 38: Raw and interpreted seismic cross-sections in time. Location of the cross-section is shown in the inset map along with boreholes and recognized faults.	54
Figure 39: Raw (a) and interpreted (b) seismic time slices at 0.4 sec. BFZ: Babaeski Fault Zone, KKFZ: Karakavak Fault Zone.	55
Figure 40: Raw (a) and interpreted (b) seismic time slices at 0.5 sec. BFZ: Babaeski Fault Zone, KKFZ: Karakavak Fault Zone.	56
Figure 41: Raw (a) and interpreted (b) seismic time slices at 1.0 sec. BFZ: Babaeski Fault Zone, KKFZ: Karakavak Fault Zone.	57
Figure 42: Raw (a) and interpreted (b) seismic time slices at 1.5 sec. BFZ: Babaeski Fault Zone, KKFZ: Karakavak Fault Zone.	58
Figure 43: a) Major structures of the study area and their rose diagrams. b) Interpretation of the structures along the strain ellipse assuming that all the	

structures are developed under N-S (perpendicular to fold axes) regional compression and E-W extension.....	61
--	----

CHAPTER 1

INTRODUCTION

1.1 Purpose and Scope

The Thrace Basin is a triangular shaped Tertiary Basin in the northwest Turkey and characterized by structures associated with strike-slip faults. The basin displays attractive prospective traps for hydrocarbon and receives much of the attention from the petroleum industry. Explorations in the basin started in early 1960s (Hoşgörmez, et al., 2005) and by the end of 1997, two small oilfields (Deveçatağı and Kuzey Osmancık) and series of gas fields (e.g. Hamitabat, Karacaoğlu, Umurca, Kandamış, and Hayrabolu) have been discovered (Coşkun, 2000). Today, the Thrace Basin has many gas producing fields. Despite the extensive exploration efforts, there are only few studies, which address the kinematics and deformation mechanism of the region in the context of its structural development.

In this study, 3D raw seismic data set collected around Babaeski Fault Zone (Perinçek, 1991) is first processed to improve the data quality (Figure 1). Then, seismic data is interpreted along with the available borehole data to map the detailed subsurface geometry of the study area. Finally, seismic interpretation is used to reveal the deformation mechanism, kinematics and structural development of the region that could be beneficial for future exploration efforts and contribute towards understanding the tectonic evolution of the central Thrace Basin, origin of the transcurrent tectonics and possible role of the North Anatolian Fault Zone in the region.

1.2 Study Area

The three dimensional seismic data set namely Temrez 3D covers approximately 269 km² of the central Thrace Basin near the Alpullu natural gas production field and lies between Babaeski to the north, Hayrabolu to the south, Uzunköprü to the west and Lüleburgaz town to the east (Figure 1). In addition, study area is bounded by major structures, such as Babaeski High and Babaeski Fault Zone (Perinçek, 1991; Coşkun, 2000).



Figure 1: Location map of the study area. Satellite image is taken from Google Earth.

1.3 Data and Method of Study

1.3.1 3D Seismic Data Acquisition

Temrez 3D seismic data was shot between 10/07/2006 – 04/10/2006 by Geofizika Krakof Sp. Z.o.o. along 20 swaths each containing 6 shot lines separated by 300 m and 6 orthogonal seismic lines with 120 channels. The channel spacing was 50 m and 12 geophones were connected to each channel. The resultant seismic data set contains 746 inlines and 636 crosslines. For the shots, alternative energy sources (dynamite and/or vibroseis) were used based on site conditions. In the field, dynamites energy source were used in areas with accessibility problems such as flood plain along the river bed. Dynamites were located at the depth between 3-5 meters. In the accessible areas 4 vibrators were used to create vibroseis source.

After the energy released into the ground, 720 channels of the swath line started to record for 8 seconds of reflected seismic energy with a sampling rate of 2 msec. This resulted in high quality seismic data where the nominal fold (the number of seismic traces sharing a common mid-point) of the array is 30 (Figure 2).

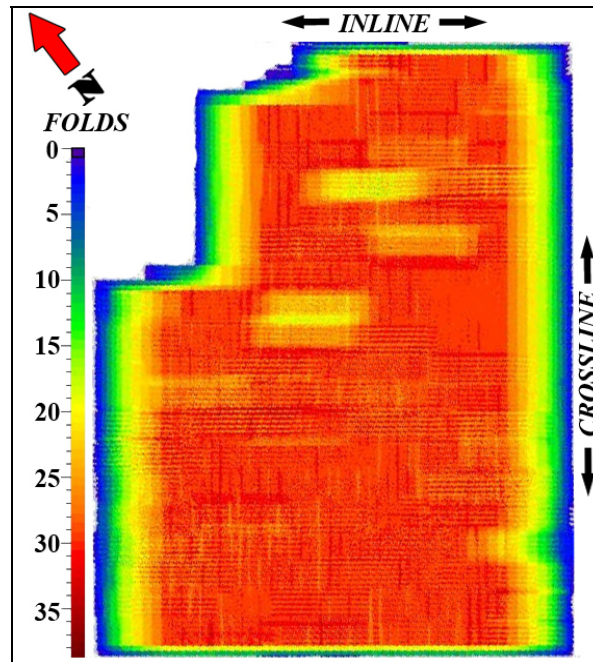


Figure 2: Fold map of the Temrez 3D survey.

1.3.2 Borehole Data

Three wells, which are Pancarköy-1, Karakavak-1, and Közpinar-1, are used in this research to understand sequence stratigraphy of the study area and to interpret stratigraphic units throughout the study area (Figure 3). Pancarköy-1 and Karakavak-1 wells are located within the survey area and have a maximum depth 4780 m and 4242 m respectively; however Közpinar-1 is located northwestward from the study area and has maximum depth 3342 m.

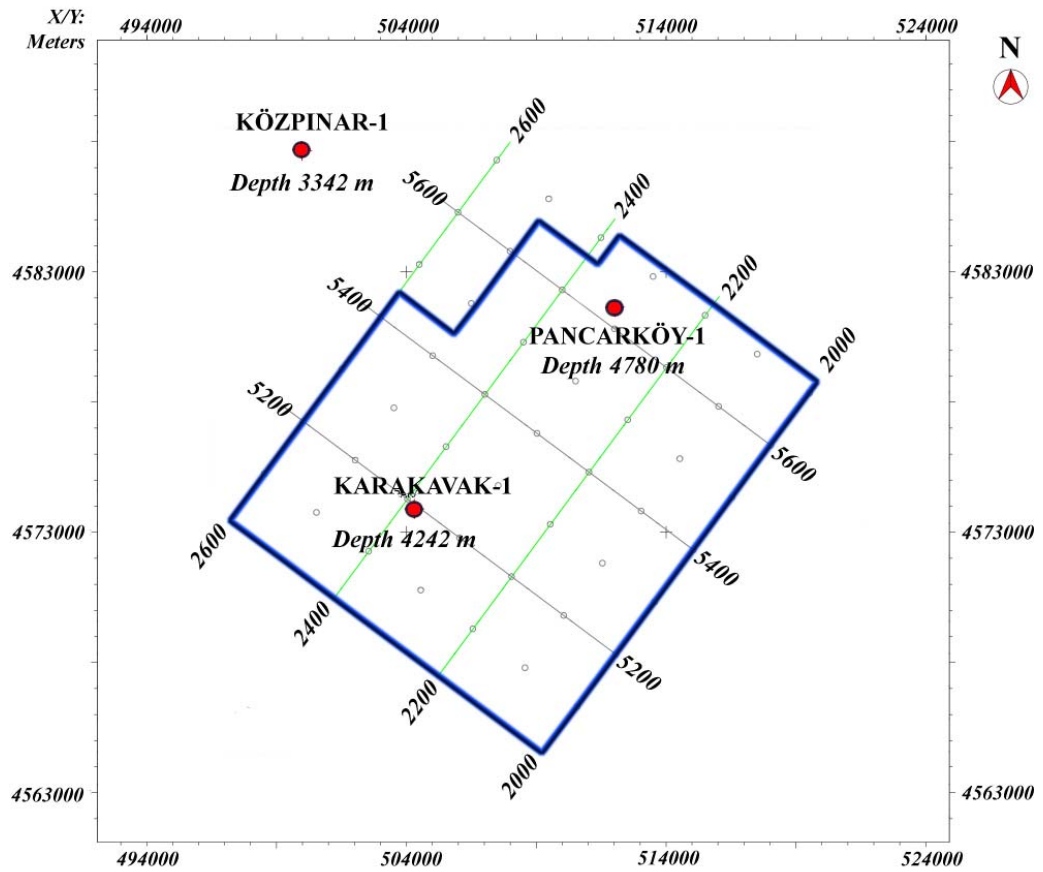


Figure 3: Map of the Temrez 3D seismic survey showing the location of wells (red circles) used in this study along with their maximum depths.

1.3.3 Seismic Processing and Interpretation

Seismic reflection data are subjected to various processing steps in order to enhance reflected signals and to present the data in a more interpretable format and filter out undesired artifacts. In this study, the raw seismic data is reprocessed to increase the signal to noise ratio and achieve the best possible seismic images of the subsurface (Figure 4). During seismic processing, the processing sequence designed by Jeoveri Processing Company is used to enhance structural interpretability while preserving original amplitude gains.

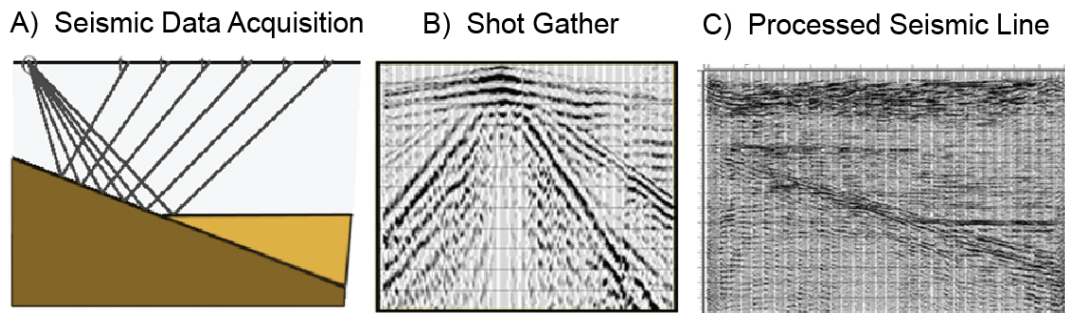


Figure 4: Schematic representation of data acquisition, initial and processed data in seismic reflection method.

After data processing, the seismic data was interpreted using SMT Kingdom Suit Software. First, processed data are loaded with well data into the SMT Kingdom Suit database. In order to correlate the seismic horizons with the stratigraphic units, the well data are converted into the time domain using velocity model. At this stage, key horizons are selected by considering known formation boundaries and reflections, which can be traced throughout the survey area. Next, reflections of selected key horizons are picked and interpreted on seismic sections in time domain. Structural elements (faults, folds, unconformities, bedding, etc.) are then interpreted by means of reflection geometries and their offsets. In the final stage, the revealed subsurface structures are used to evaluate the basin geometry, deformation style, and tectonic evolution.

1.4 Previous Studies

A number of scientific and commercial studies have been conducted in the Thrace Basin since 1947.

Pamir and Baykal (1947) pointed out that the basement of the Thrace Basin is the Strandja Massif and is composed of metamorphic rocks.

Akartuna (1953) and Arıç (1955) provided the first local geological map of the southern Thrace Basin.

Holmes (1961) established the lithostratigraphical units with type section of the region. In addition, he differentiated the transgressive and regressive sections using field observations.

Druitt (1961) is one of the first prospect-oriented worker who evaluated petroleum potential of the basin. He emphasized the importance of the fault related structures, which have turned into discoveries in the recent years (e.g. Hamitabat and Umurca Fields).

Kemper (1961) worked on the evolution of the Early Eocene period of the Kırklareli region and presented detailed depositional and petrophysical properties of the Kırklareli Limestone.

Gökçen (1971 and 1973) studied the lithological and sedimentological properties of the Karaağaç, Fıçitepe and Gaziköy formations and revealed a detailed Paleogene stratigraphy of the region.

Keskin (1971 and 1974) carried out the first attempt to construct the detailed geological and depositional model of the Trace basin. Also, Keskin reorganized the Keşan, Yenimuhacır and Ergene Groups.

Ediger and Batı (1987) carried out stratigraphical and sedimentological investigations using well data to understand the paleoenvironmental, stratigraphical and geological aspects of the Tertiary section of the basin. Hence, they focused on identification of the source and reservoir rocks and their depositional systems.

Perinçek (1991) introduced effects and implications of the North Anatolian Fault System on the tectonic evolution of the Thrace Basin. In the region, he defined three major fault systems, namely, Kırklareli, Lüleburgaz and Babaeski Fault Zones.

Burkan (1991) worked on the evaluation of organic geochemical characteristics of the Tertiary deposits. Moreover, he demonstrated the petroleum generation potential of each source rock unit and ranked them according to their generation potential and maturity.

Turgut et al. (1991) performed regional scale correlations and established a correlation chart based on well logs and seismic data.

Atalık (1992) studied the depositional system of the Osmancık formation based on well data and seismic reflection profiles.

Based on outcrops and well data, Görür and Okay (1996) claimed that the Thrace Basin is located on the Strandja Zone and evolved as a fore-arc basin during the Paleogene.

Based on well data and seismic profiles, Coşkun (1997 and 2000) stated that the Thrace Basin is an intermontane trough, surrounded by the granitic and metamorphic rocks of the Istranca and Rhodope Massifs.

Turgut (1997) studied the depositional sequences and hydrocarbon potential of the basin. He constructed sequence stratigraphy of the Eastern Thrace, which was the first study accomplished based on identified systems tracts.

Yaltırak, et al. (1998) interpreted the tectonic evolution of the Gulf of Saros using seismic and geologic data.

Sakınç et al. (1999) analyzed the tectonic evolution of the Thrace Basin by reconstructing its palaeogeography during the Neogene time.

Turgut and Eseller (2000) integrate an extensive reflection seismic data set with well and outcrops information to develop the sequence stratigraphic framework and analyzed the evolution of the eastern Thrace Basin to evaluate its hydrocarbon potential.

Yaltırak (2002) integrated geological data with the marine seismic profiles to reveal the tectonic evolution of the Marmara Sea and its surroundings.

Based on shallow marine seismic data and onshore geological field observations, Yaltırak and Alpar (2002) analyzed the kinematics and tectonic evolution of the Ganos Fault System.

Elmas (2003) studied neo-tectonic evolution of the basins in Marmara region based on field observations from the different morpho-tectonic units, geological and geophysical data.

Hoşgörmez and Yalçın (2005) determined the maturation and gas generation history of three possible source rocks in respective drainage areas of the different gas fields in the Thrace Basin.

Huvaz et al. (2005) studied the vitrinite reflectance patterns of wells located in the Thrace Basin to reveal the thermal history and analyzed the chronostratigraphy of the basin from seismic data.

Zattin et al. (2005) made apatite fission-track analysis and suggested that the present-day Ganos Fault follows the trace of a pre-existing structural discontinuity active by late Oligocene time.

Kaymakçı et al. (2007) shed some light on the tectonic development of NW Turkey by integrating the results of paleomagnetic measurements and radiometric dating of basaltic lavas, and noted possible relationships between regional tectonic activity and the development of mantle-derived mafic alkaline lavas during the Late Miocene.

Siyako and Huvaz (2007) described the Eocene stratigraphic evolution of the Thrace Basin using the seismic data profiles, well data, and outcrop information.

Sunal (2008) studied in the geology of metamorphic rocks in the Strandja Massif by detail geological mapping, petrography, petrology, and U-Pb and Rb-Sr geochronology.

S nnet iođlu (2008) studied the depositional history of the Upper Eocene sedimentary succession in a sequence stratigraphic approach in the northwest Thrace Basin.

 slamođlu et al. (2010) studied the stratigraphic succession and paleontological content of Oligocene deposits to analyze depositional environments in terms of paleoecology and paleogeography.

Okay et al. (2010) studied the ophiolitic basement of the Trace basin around řark y which includes erosional remnants of lower Eocene series, upper Eocene - lower Oligocene olistostromal sequence with ophiolitic clasts and large Eocene limestone blocks.

 zcan et al. (2010) established the biostratigraphy of the Eocene marine sequence in the southern part of the Trace basin and identified a shallow marine transgressive Diřbudak sequence located below the Sođucak formation.

Yılmaz et al. (2010) discussed the evolution and development of the morphotectonic structures in the Marmara region.

CHAPTER 2

GEOLOGY

2.1 Regional Stratigraphy

The unit exposed within and around the Thrace Basin can be divided into two as 1) pre-Eocene basement units and 2) Eocene to Recent basin infill.

The basement of the Thrace Basin consists of five different units: (1) Strandja-Rhodope Massif which crops out in the northern part of the basin; (2) Paleozoic and Triassic Istanbul Block sequences crops out in the east of the basin; (3) Upper Cretaceous island-arc volcanics (Yemişliçay Formation); (4) Early Cretaceous-Paleocene Çetmi Opholitic Mélange exposed along the southern margin of the basin and is delimited by the North Anatolian Fault Zone within the Gallipoli Peninsula and Mürefte-Şarköy region; and (5) pre-Jurassic lithologies comprising the Kazdağ Group metamorphics, Karakaya Complex and post-Triassic cover sequences of the Sakarya Continent exposed in the southern part of the basin and Marmara islands (Huvaz, 2005; Siyako, et al., 2007).

The basin infill units in the central Thrace Basin reaches up to 9000 m along a SE-NW axis extending from Marmara Ereğlisi in the east along the Marmara Sea coastline to Babaeski near Greco-Turkish boundary (Figure 5). Most of the sequence was deposited in the Eocene-Oligocene time interval and comprises mainly siliciclastic rocks and intercalated shallow marine carbonates (Siyako, et al., 2007; Okay, et al., 2010). In the northeast along the Strandja Massif, the sequence is characterized by shallow marine deposits and grades southwestwards into the deeper marine limestones, marls and turbidites (Okay, et al., 2010). The

Eocene shallow-marine deposits in the south near the Şarköy and Mecidiye are regarded as the manifestation of southern shelf of the basin (Turgut, et al., 1991; Tüysüz, et al., 1998; Okay, et al., 2010).

The basin infill is accumulated during two major phases of subsidence. Middle Eocene is characterized by fast subsidence and high sedimentation rate (Sakinç, et al., 1999; Siyako, et al., 2007). The units deposited during this period are characterized by a transgressive cycle (Figure 6) that initially focused mainly in the central part of the basin and later it extended towards the southwest to northeast direction (Figure 7) (Keskin, 1974; Turgut, et al., 2000; Siyako, et al., 2007). Reefal to shallow marine sediments were deposited on the shelves and paleohighs while in the deep parts mainly turbiditic clastics were deposited as manifested by alteration of shale, claystones, siltstones and fine-grained poorly sorted sandstones (Turgut, et al., 2000). In addition, intermediate andesitic volcanism introduced considerable amounts of volcanic ash into the basin during this time (Turgut, et al., 1991).

Middle Eocene transgression was followed by a regressive cycle during Early Oligocene-Early Miocene time interval (Keskin, 1974). Dominant facies were fluvial, lagoonal and shallow marine in character (Figure 6) and characterized by alteration of claystones with sandstones and siltstones (Keskin, 1974). This time corresponds to the final stage of subsidence and fast deposition in the basin (Turgut, et al., 1991) that was followed in the southern margin by Early Miocene volcanics.

Middle to Late Miocene period was associated with relatively slow burial and deposition rate (Siyako, et al., 2007). During this time the Thrace Basin was the locus of continental siliciclastic deposition composed of fine- to coarse-grained fluvio-lacustrine deposits in the basin center while the margins were dominated by near shore marine deposits. All of these units unconformably overlie the older units (Figures 6 and 7) (Keskin, 1974).

Pliocene to Recent deposits in the basin are dominated by fluvial system which are derived mainly from Strandja Massif in the north and accumulated along the active drainage system as alluvial plain deposits (Figure 5).

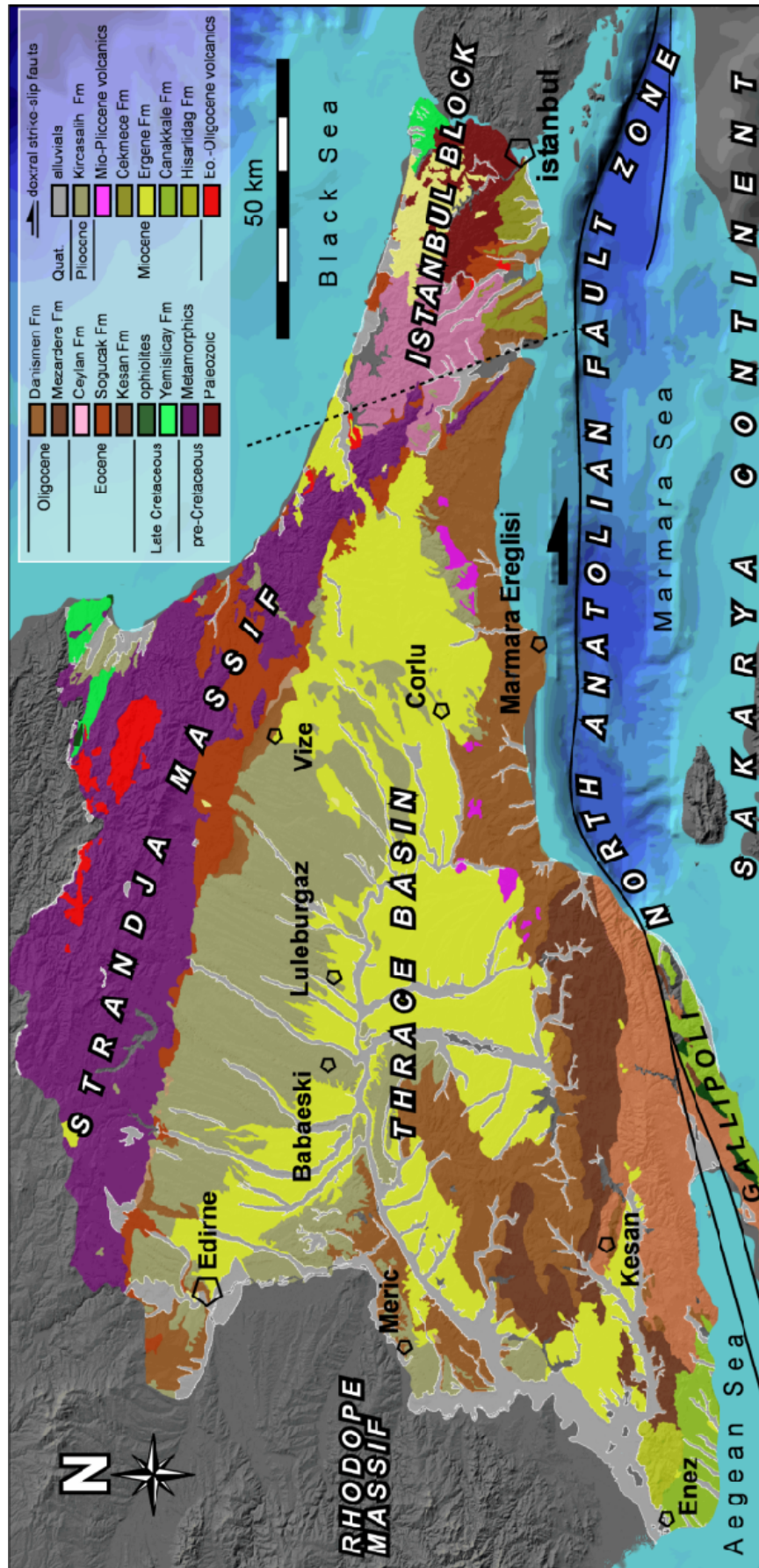


Figure 5: Geological map of the Thrace Basin taken from Siyako, et al. (2007).

SYSTEM	AGE	UNITS		LITHOLOGY	DEPOSITIONAL ENVIRONMENT
TERTIARY	PLIOCENE	KIRCASALIH FORMATION			FLUVIAL
	MIOCENE	ÇANAKKALE FM.	ERGENE FM.		NEAR SHORE, LAKE FLUVIAL
		HISARLIDAG FM.			VOLCANICS
	OLIGOCENE	YENIMUHACIR GROUP	DANISMEN FM.		DELTAIC SYSTEM
			OSMANCIK FM.		DELTA PLAIN LAKE
			MEZARDERE FM.		DELTA FRONT
	EOCENE	KESAN FM.	CEYLAN FM.		PRODELTA
			SOĞUCAK FM. KOYUNBABA FM.		PROXIMAL-DISTAL TURBIDITES
		GAZİKÖY FM.	FICITEPE FM.		SHALLOW TO DEEP MARINE SHALLOW MARINE
			KARAAĞAÇ FM.		FLUVIAL
PALEOZOIC MESOZOIC			HAMİTABAT FM.		PROXIMAL-DISTAL TURBIDITES FLUVIAL PROX-DISTAL TURBIDITES
		BASEMENT			

Figure 6: Generalized lithostratigraphic section of the Thrace Basin taken from Sünnetçioğlu (2008).

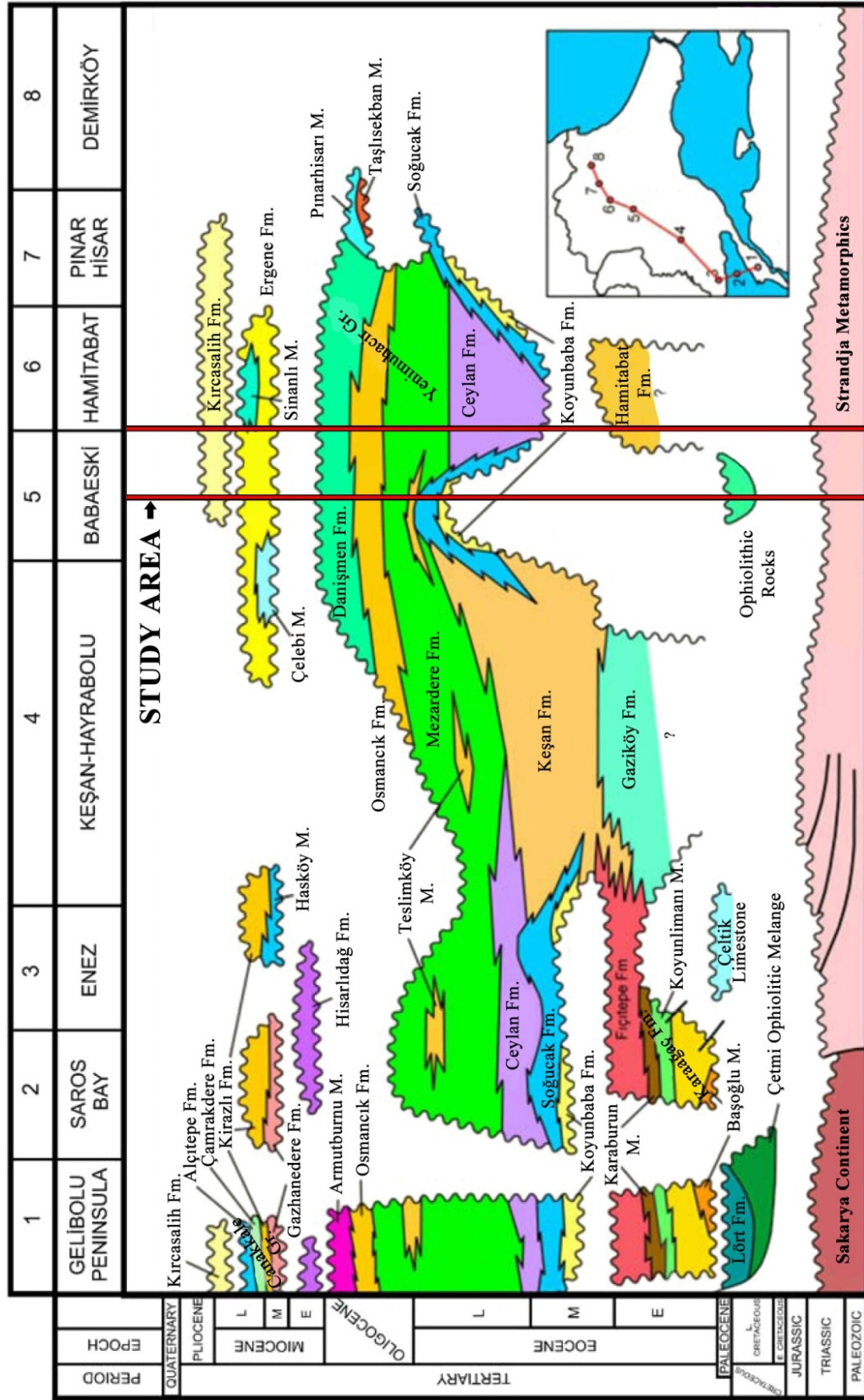


Figure 7: Generalized chronostratigraphic chart of the Thrace Basin taken from Sünnetçiöğlu (2008). Numbers at the top of the figure correspond to the locations shown in the inset map.

2.2 Regional Tectonic Structures

The major structures in the region are mainly dextral strike-slip fault systems. In the south, Thrace basin is bounded by the active Ganos fault, which constitutes the offshore section of the North Anatolian Fault Zone (Yaltrak and Alpar, 2002). In the north, the Thrace Fault Zone is one of the most important structures (Perinçek 1991). It trends NW-SE direction and extends for about 130 km through the northern margin of the Thrace Basin (Figure 8).

Perinçek (1991) suggested that the Thrace Fault Zone is an inactive northern splay of the North Anatolian Fault Zone and it shows most of the characteristic features of strike-slip faults on seismic sections: such as releasing bends; restraining bends, positive and negative flower structures (Figure 8). However, Yaltrak (2002) proposed that the Thrace Fault was western continuation of Thrace-Eskişehir Fault zone and defined the early neotectonic signature during Early Miocene to Early Pliocene interval in northwest Turkey.

Within the Thrace Basin, the Thrace Fault Zone is divided into three major sub-zones: 1) Kırklareli Fault Zone, 2) Lüleburgaz Fault Zone, and 3) Babaeski Fault Zone (Figure 9).

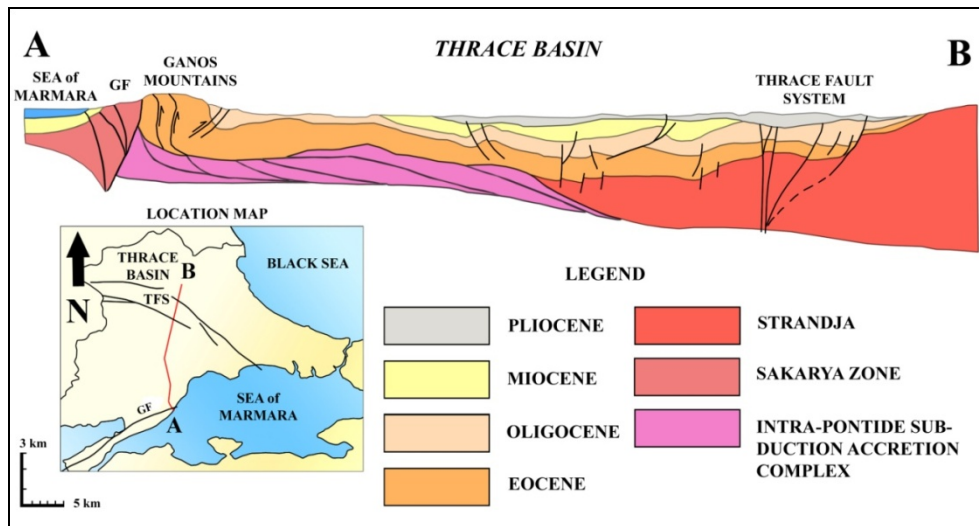


Figure 8: The geological cross-section depicting major structures of the Thrace Basin. Location of the section is indicated in the inset map. TFS, Thrace Fault System; GF, Ganos Fault; (Görür, et al., 1996).

Although, the inception age of the Thrace Fault Zone is debated, it is generally accepted that it was commenced during the late Middle Miocene (Perinçek, 1991) and deactivated at the end of Early Pliocene after the commencement of the North Anatolian Fault Zone as a through going lithospheric structure that marks the beginning of neotectonic period in Turkey. According to Yalırak (2002) and Okay et al. (2000) this gave way to deactivation and separation of Thrace-Eskişehir Fault Zone into two sub branches (Figure 9).

Recently, the lineament that trends subparallel to Ganos fault between Keşan and Çorlu districts have been proposed as the dextral strike-slip Tekirdağ fault by Kaymakçı et al. (2007) based on morphological features. The Tekirdağ fault has no recent seismic activity and was active probably prior to mid-Pliocene time. Paleomagnetic data indicate large clockwise rotations during Late Miocene within the shear zone delaminated by the Tekirdağ Fault in the north and Ganos Fault in the south. (Kaymakçı et al., 2007).

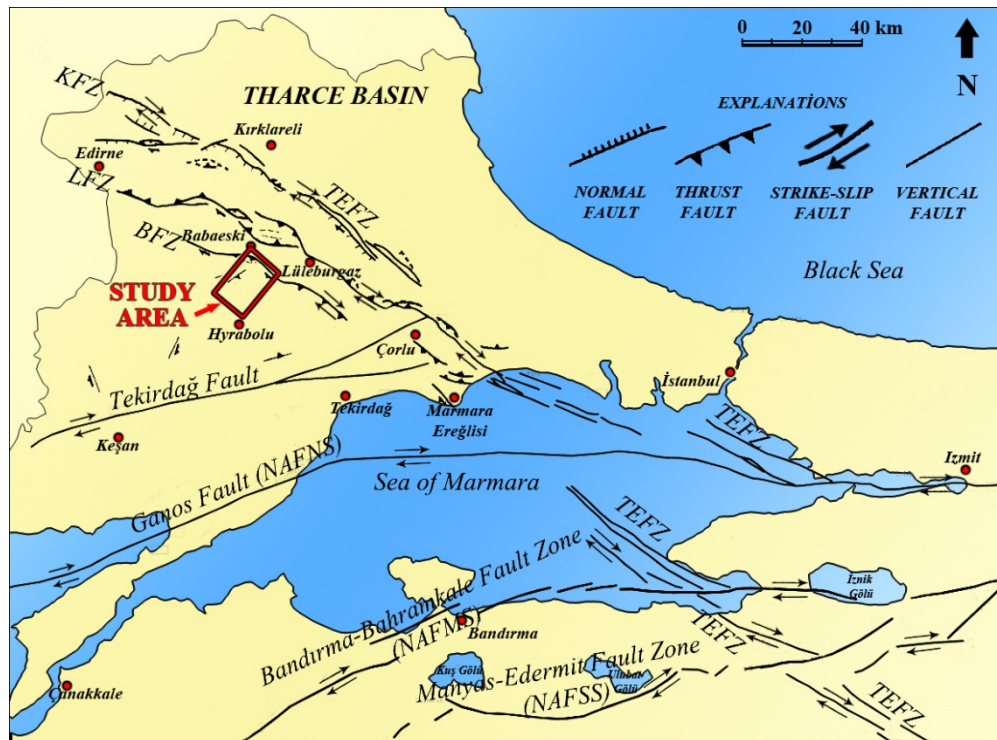


Figure 9: Structural map of the northwest Turkey (Yalırak 2002, Kaymakçı et al. 2007). TEFZ: Thrace-Eskişehir Fault Zone, KFZ: Kırklareli Fault Zone, LFZ: Lüleburgaz Fault Zone, BFZ: Babaeski Fault Zone, NAFNS: Northern Strand, NAFMS: Middle Strand, NAFSS: Southern Strand of the North Anatolian Fault.

2.3 Geological Evolution

The tectonic origin and evolution of the Thrace Basin is under debate. For example Görür and Okay (1996) proposed that the basin has fore arc origin based on outcrop and borehole data. According to this scenario during the Eocene, the Intra-Pontide Ocean (IPO) was still open and its eastern part might have been reduced to a narrow canal, due to convergence between Istanbul Block in the north and Sakarya Continent in the south (Görür, et al., 1996). This convergence gave way to collision of Sakarya Continent with the Istanbul Block during the Early Eocene, which obliterated the eastern part of the IPO (Figure 8). During this time interval and much of the Eocene, the western part of the IPO was still open and subducting northwards below the Strandja Massif (Görür, et al., 1996). This subduction accompanied with Eocene extension that led to rifting of the Strandja zone and opening of the Thrace Basin (Görür, et al., 1996) which was closed completely during the Oligocene.

On the other hand, Keskin (1974), Perinçek (1991), and Coşkun (2000) proposed that during the Late Cretaceous and Paleocene, the region was site of intense convergence and compression characterized by complex thrusting and metamorphism due to convergence between Eurasia in the north and Tauride-Menderes Block in the south. They further claimed that convergence and suturing lasted until the Eocene in the region and is followed by a phase of extension in the Eocene-Oligocene during which much of the infill of the Thrace basin was deposited. Similarly, based on seismic and well data Siyako (2007) claimed that the fore arc nature and closure of the IPO took place much earlier than Eocene contrary to Görür and Okay (1996) and Görür et al. (1996). He claimed that during the Eocene-Oligocene it was an intermontane basin.

2.4 Local Stratigraphy

Ceylan Group is the oldest basin fill unit in the study area. It comprises Hamitabat, Koyunbaba, Soğucak and Ceylan formations (Figure 10). Although, they have local unconformable relationships, laterally and vertically these units partly grades into each other.

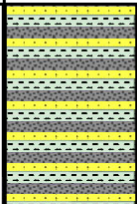
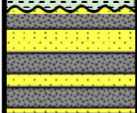
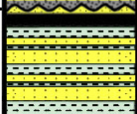
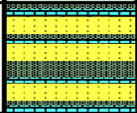
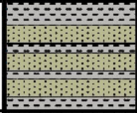
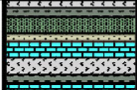

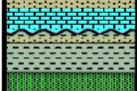


CHRONO-STRATIGRAPHY				THICKNESS (m)	LITHO-STRATIGRAPHY	
TERTIARY	PLIOCENE	KIRCASALIĞ FM.	ERGENE GROUP	~100		Nodular limestone-clay alteration, sand intercalations are frequent within the clay
	MIOCENE	ERGENE FM.				Unconsolidated conglomerates, sandstones and claystones and overlies all the order series with a distinct erosional unconformity of basin wide extent
	OLIGOCENE	DANIŞMEN FM.		0-700		Greenish gray shales, claystones and coals interbedded with light gray to yellowish brown and cross-bedded fine grained sandstones and siltstones
		OSMANCIK FM.		~1900		Fine to coarse pebbly grained sandstones, interbedded with greenish brown shales and siltstones
		MEZARDERE FM.		~1450		Fine to coarse pebbly grained sandstones, interbedded with greenish brown shales and siltstones
	EOCENE	CEYLAN FM.	CEYLAN GROUP	500-3000		Interbedded dark gray to greenish gray shales, marlstones, siltstones, argillaceous limestones with tuffaceous and volcanic layers
		SOĞUCAK FM.				Gray to dark gray argillaceous limestones and marls
		KOYUNBABA FM.				Pebbles, sandstones, marl, clay, carbonate and mega blocks of basement
		HAMİTABAT FM.				Light gray sandstones, greenish gray siltstones and dark gray shales, pebbly sandstones and conglomeratic wedges
	PALEOZOIC MESOZOIC	BASEMENT				Metamorphic and igneous rocks.

Figure 10: The stratigraphic columnar section of the study area after Turgut et al. (2000). Note that thickness information are derived from available borehole data.

Well cuttings, cores, well logs and seismic data indicate that the Hamitabat Formation overlies the Strandja Metamorphics nonconformably. It consists of interbedded gray colored sandstones, siltstones and dark gray colored shales (Huvaz, 2005). The deposition environment varies from shallow marine to deep marine. Most of the sandstone lithologies are deposited as distal, proximal and inter-channel turbidities in deep marine environment. However, extensive burrowing, small-scale current ripples and organic production represent a shallow marine environment (Sünnetçioğlu, 2008). The age of the Hamitabat Formation according to Ediger, et al. (1987) is of Middle to Late Eocene.

The Hamitabat Formation is unconformably overlain by the Koyunbaba Formation, which was identified first by Krausert and Malal (1957). Koyunbaba Formation also overlies the metamorphic rocks of the Strandja Massif nonconformably and vertically and laterally grades into the Soğucak Formation (Sünnetçioğlu, 2008). It is composed of pebbles, sandstones, marl, clay, carbonate and mega blocks derived from the basement (Sünnetçioğlu, 2008). The deposition starts with basal conglomerates and grades upwards into pebbly sandstone, siltstone, and sandy limestone facies. These lithologies are products of shallow marine environment facilitated by the Middle to Late Eocene transgression (Turgut, et al., 2000).

Soğucak Formation was firstly discovered by Holmes (1961). Locally it unconformably overlies the Hamitabat Formation in the deep part of the basin and conformably overlies Koyunbaba Formation in the southern part of the basin. It consists of white to buff shallow marine reefal limestones and skeletal platform carbonates of massive appearance where it overlies the Koyunbaba Formation and gray to dark gray argillaceous limestones and marls where it overlies the Hamitabat Formation (Sünnetçioğlu, 2008). Microfacie studies reveal that the Soğucak Formation developed in the various environments extending from open shelf, shelf margin and restricted shelf to lagoon (Atalık, 1987). According to Atalık (1992), the age of the Soğucak Formation ranges between late Middle Eocene to the early Oligocene (Figure 10) whereas it is Late Eocene according to Sünnetçioğlu (2008).

Ceylan Formation was identified by Ünal (1967) and it conformably overlies the Soğucak Formation and consists of interbedded dark gray to greenish shales, marlstones, siltstones, argillaceous micritic limestones, very fine-grained sandstones, tuffs and variegated volcanics (Turgut, et al., 2000). The deposition environment varies from shallow marine to deep marine (Sünnetçioğlu, 2008). Ceylan Formation shows great thickness variations and its shales shows good source rock properties (Huvaz, 2005). According to the studies provided by Gerharg and Alisan (1987), the age of the Ceylan Formation is of Middle to Late Eocene.

Mezardere Formation was first described by Ünal (1967). It overlies the Ceylan Formation conformably (Figure 10) and consists of interbedded greenish gray to bluish gray shales, siltstones and fine-grained sandstones (Turgut, et al., 2000). Intermittent tuffaceous interbeds are also present towards the bottom of the formation. The greenish and bluish gray shales have a waxy texture and contain abundant organic matter (Turgut, et al., 1991, 2000). Dominant shale lithologies indicate that the Mezardere Formation was deposited in the shallow to moderately deep marine environment as a part of the Yenimuhacir Group (Sünnetçioğlu, 2008). Based on paleontologic data, the age of the Mezardere Formation is given as Late Eocene-Early Oligocene (Gerhard, et al., 1987).

Osmancık Formation was introduced by Holmes (1961). It overlies the Mezardere Formation conformably in the basinal areas (Figure 10). It consists of fine to coarse pebbly grained sandstones with abundant cross-bedding, interbedded with greenish brown shales and siltstones thought to be deposited in a deltaic environment (Atalık, 1987). In the seismic sections, the shallowest portions correspond to the boundary between terrestrial and marine environments, and deepest portions of the unit corresponds to the boundary between nearshore and offshore environments (Sünnetçioğlu, 2008). Based on the stratigraphic relations and paleontologic data, the age of Osmancık Formation is Early to Late Oligocene (Gerhard, et al., 1987; Atalık, 1992).

Danişmen Formation was identified by Boer (1954). It overlies the Osmancık Formation conformably (Figure 10) and consists of greenish gray shales, claystones and coals interbedded with light gray to yellowish brown and cross-bedded, fine-grained sandstones and siltstones (Sünnetçioğlu, 2008). Occasionally, conglomeratic wedges and tuffite intercalations are also present. Laminated light and dark colored bands, and abundant plant debris and fish scales within the shales are characteristic features of this formation (Turgut, et al., 2000). These lithologies are the products of lagoon, swamp, flood plain and fluvial environments. A Late Oligocene - Early Miocene age has been assigned to the Danışmen Formation by Gerhard and Alisan (1987) and Atalık (1992).

Mio-Pliocene Ergene Group comprises the Ergene and Kırçasahil formations (Figure 10). Ergene Formation, which is composed of conglomerates, sandstones and claystones of alluvial origin, was deposited in a fluvial environment during Middle to Late Miocene time and overlies all the older sequences with a distinct erosional unconformity of basin-wide extent (Turgut et al., 2000). The youngest Tertiary unit in the study area is the Pliocene Kırçasalih Formation, which overlies the Ergene Formation unconformably. This unit is also derived from fluvial environment and consists of partly unconsolidated conglomerates, sandstones and siltstones derived from fluvial environment (Siyako et al., 2007).

In this study, basement; Ceylan Group that includes Koyunbaba, Soğucak and Ceylan formations; Mezardere; Osmancık; Danişmen formations and Ergene Group that includes Ergene and Kırçasalih formations are identified and interpreted in the seismic sections by correlating borehole data from three wells located within or nearby the study area. Note that basement rocks, Soğucak and Koyunbaba formations are only encountered in the Kozpınar 1 well located outside of the study area while the Pancarköy 1 and Karakavak 1 wells within the study area cut down to the Ceylan formation (Figure 11).

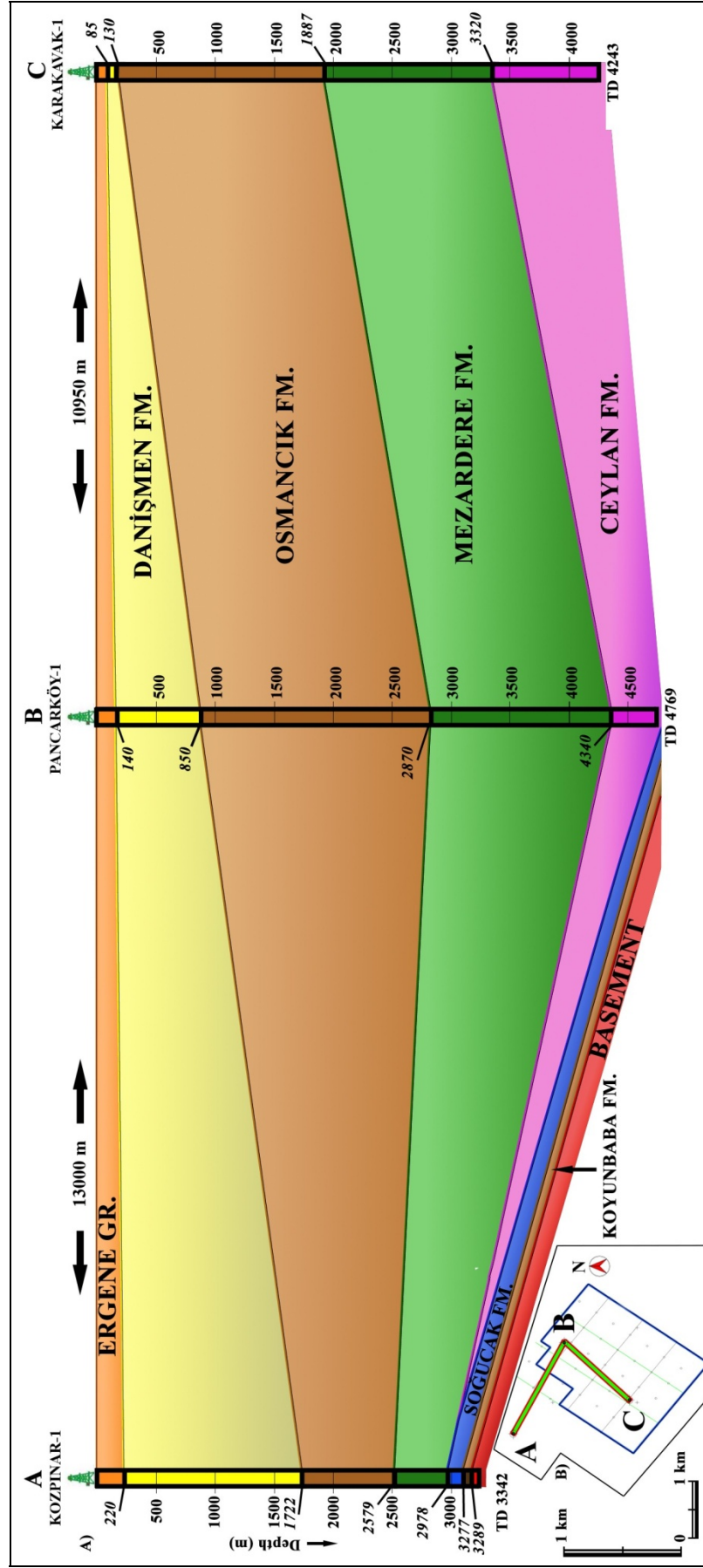


Figure 11: a) Well log correlation along transects running between boreholes used in the study area. **b)** Map showing the location of the section. TD, Total depth;

2.5 Local Tectonic Structures

The study area is covered by Pliocene age Kırcaali Formation and Quaternary alluvial deposits (Figure 12). Therefore, the tectonic structures of the basin that are older than these cover units are mainly based on seismic and borehole data.

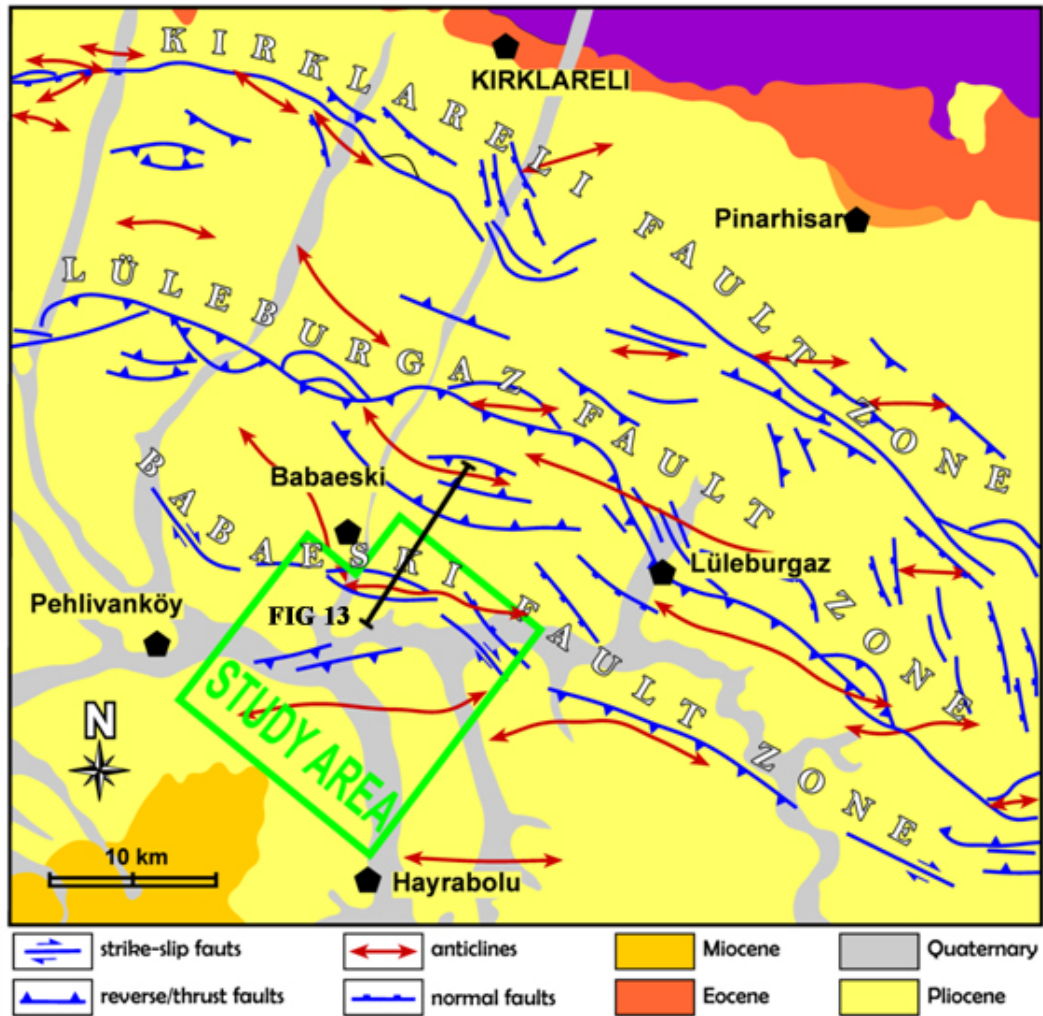


Figure 12: The map showing the geology, structural settings and location of the study area (redrawn from Perinçek 1991).

In the north, the branches of the Trace Faults System including Kırklareli, Lüleburgaz and Babaeski fault zones forms a structural complexity and corresponds with a major Late Oligocene age paleohigh known as the Kuleli-Babaeski High. Along the branches of the Trace Fault System, the region displays a transpressional character represented by NW-SE trending oblique strike-slip faults with large reverse component and series of fault bounded anticlines with trends ranging between NW-SE and W-E (Figure 12).

The study area where Temrez 3D seismic data is collected lies between Babaeski and Hayrabolu districts and includes the NW-SE trending Babaeski Fault Zone (Perinçek, 1991) that is marked by the presence of positive flower structure and fault-related anticlines recognized on 2D seismic profiles (Figure 13). Although, Perincek (1991) discussed Kırklareli and Lüleburgaz Fault Zones in detail, Babaeski Fault Zone was not discussed in detail due to limited seismic data at that time. In this study, in addition to structures proposed by Perinçek (1991), a number of newly recognized faults and folds has been analyzed and interpreted using recently acquired Temrez 3D seismic data.

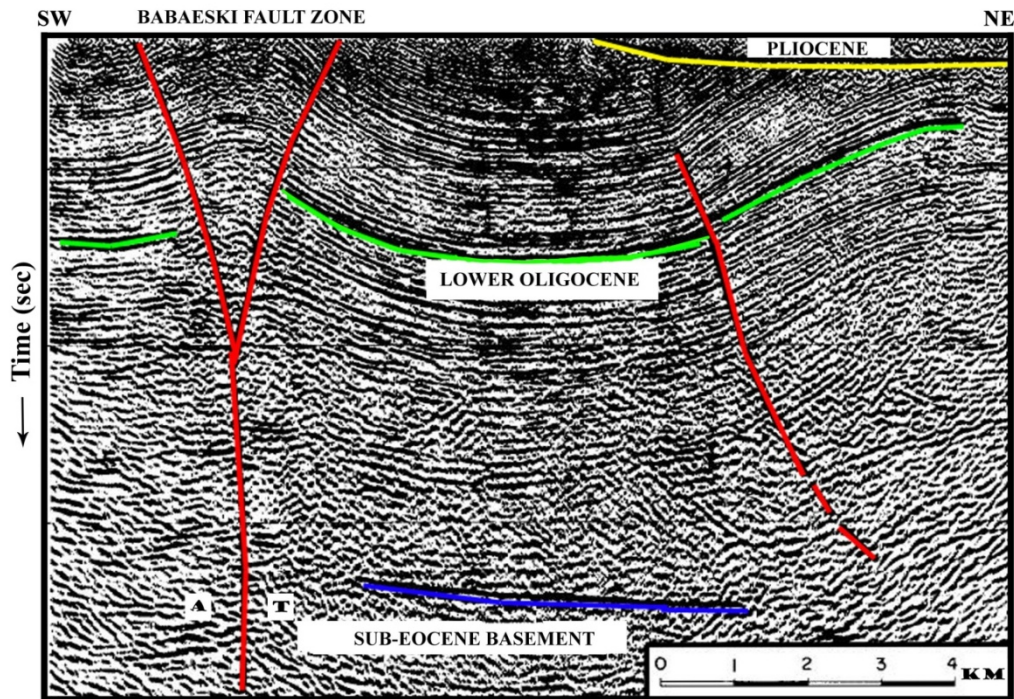


Figure 13: The interpreted 2D seismic section showing the positive flower structure along the Babaeski Fault Zone (taken from Perinçek, 1991). Location of the seismic section is shown in Figure 12.

CHAPTER 3

SEISMIC DATA PROCESSING

In order to improve seismic data quality needed for interpretation, Temrez 3D seismic data that was previously processed in the field, is re-processed during this study by using Paradigm Focus Software of Jeoven Company. In this chapter, each step of the used seismic data re-processing procedure (Figure 14) will be discussed in detail.

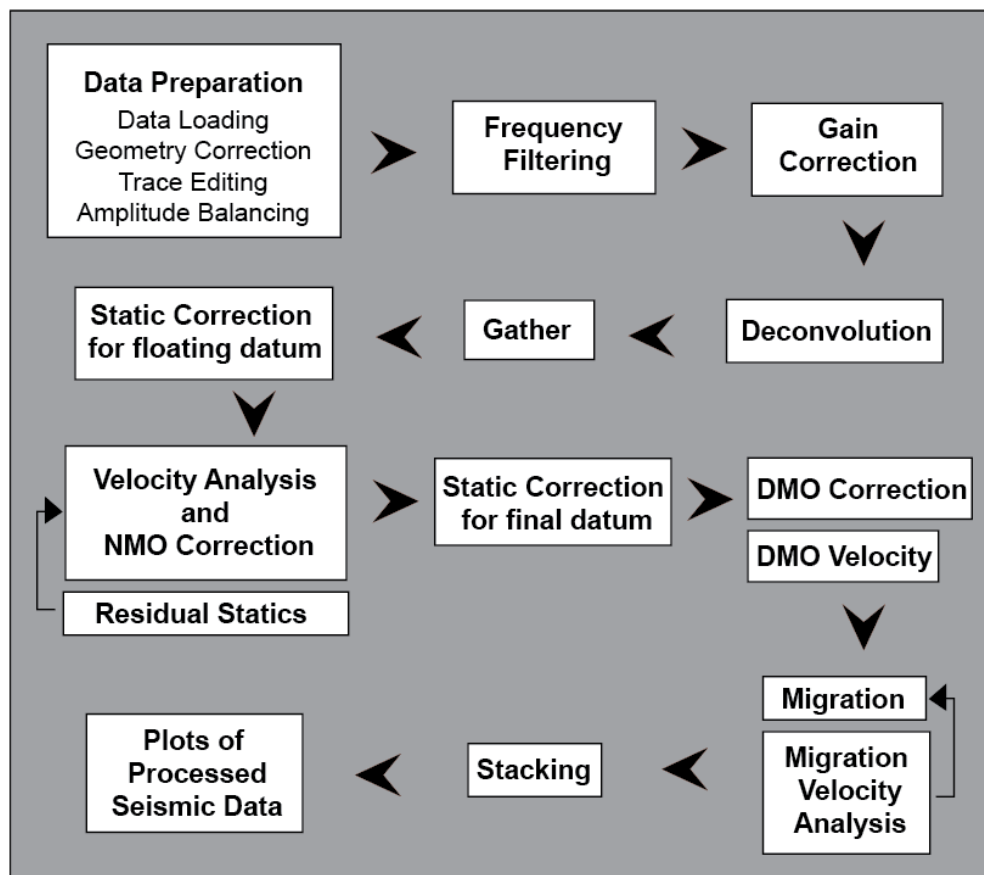


Figure 14: Seismic data re-processing sequence used in this study.

3.1 Data Preparation

Data preparation step includes data loading, geometry correction, trace editing and amplitude balancing.

During data loading, the raw seismic data collected in the field is transcribed into internal format that can be processed in Focus Software. Consequently, geometry correction is applied to construct shooting geometry of the seismic data, performing calculations based on field parameters to establish the correct geographical locations of the shots, the geophones, and the common depth points (Figure 15).

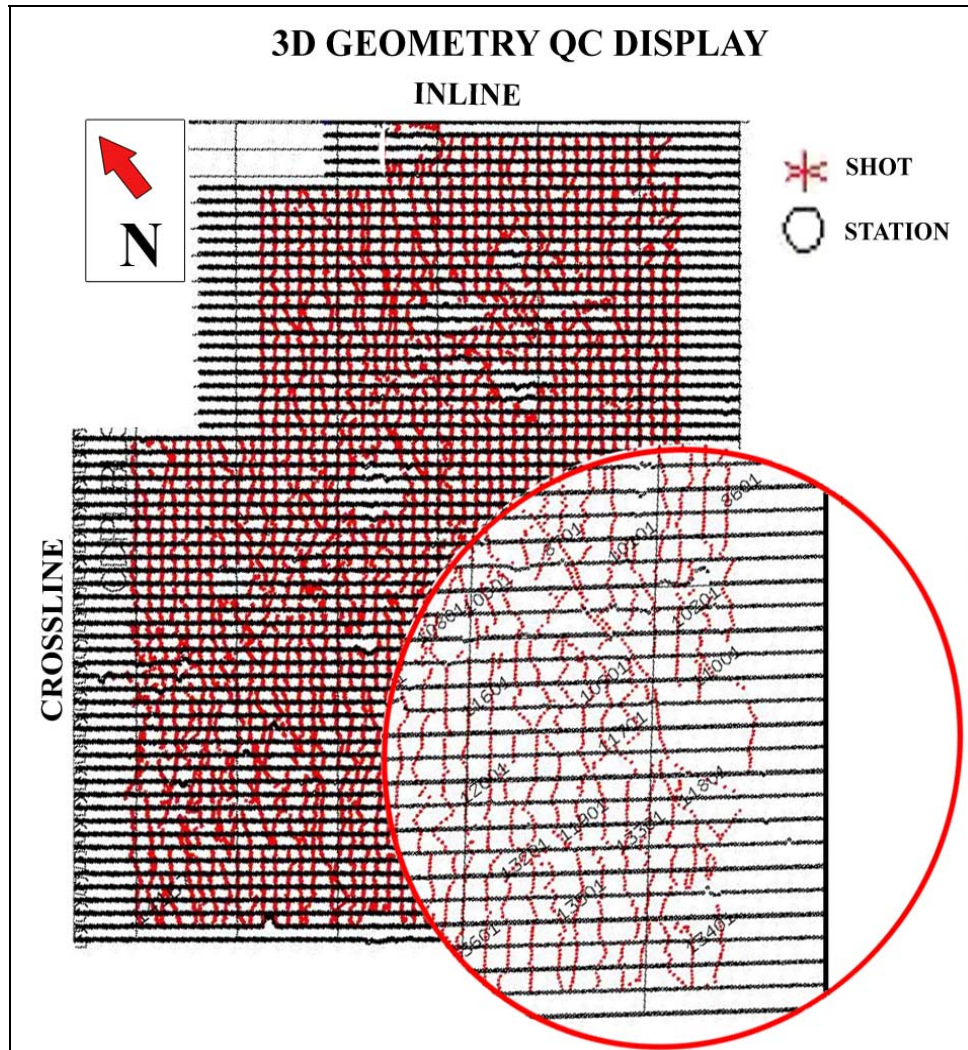


Figure 15: Quality Control of the 3D seismic data geometry.

The raw shot gathers are later checked for the presence of reversed, zero and noisy traces which are edited or removed from the data set (Figure 16a).

The near surface irregularities using two different source types brings up some differences in surface consistency meaning that vibrator and dynamite energy sources have different gain level. To compensate this problem, surface consistent amplitude balancing that calculates scaling factors for each trace using the bias, shot, geophone and offset components is applied to the data set.

3.2 Frequency Filtering

In order to remove high frequency noise and low frequency ground roll, Temrez 3D seismic data is first converted from time domain to frequency domain using Fourier Transformation that decomposes signals into a series of sine (or cosine) waves with different amplitude and phase. Then, unwanted high and low frequencies are filtered out using high-pass and low pass filters to the data in frequency domain (Figure 16b).

3.3 Gain correction

Amplitudes of the reflections decay as distance from the energy source increases due to geometric spreading, attenuation and scattering. Therefore, amplitudes of deep reflections are weak compared to initial reflections, which dominate the seismic section (Fig 16b). In order to make deeper arrivals visible, the gain correction, which accounts for the energy loss due to geometric spreading, is applied to the Temrez 3D seismic data. As a result, the reflected arrivals at different depths became equalized in amplitude allowing us to analyze deep reflections with higher signal to noise ratio (Figure 16c).

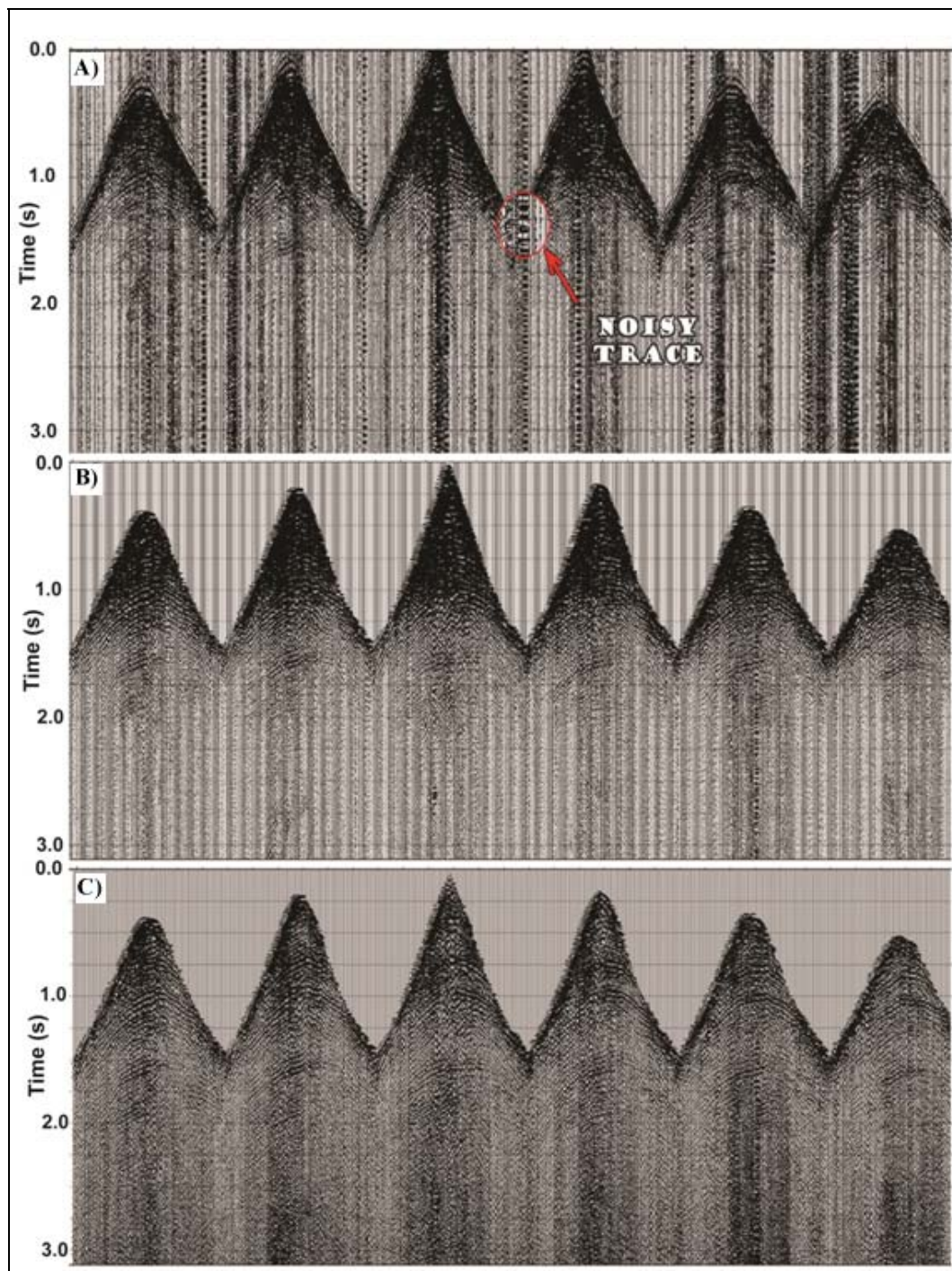


Figure 16: a) Raw shot gathers. b) Shot gathers after trace editing, surface consistent amplitude balancing and frequency filtering. c) Shot gathers after gain correction.

3.4 Deconvolution

The seismic traces that are recorded in the field depend on reflection coefficient of layers and the seismic wavelet that is set by the source. Thus, seismic trace is a convolution of the reflection coefficient and wavelet. Deconvolution (inverse filtering) is a data processing step that is used to undo the effects of previous convolution to get back the reflectivity of layers. In reflection data processing, there are different deconvolution techniques, each designed to remove some specific effects. In this study, surface-consistent deconvolution filters are designed for Temrez 3D seismic data according to the Wiener-Levinson auto-correlation algorithm, which also compensates variable shot signatures, irregular geophone coupling and attenuation of high frequencies at long offsets.

Energy generated by seismic sources has a finite duration and contain several oscillations, which causes reflections to interfere with each other, making it difficult to identify individual reflections. Therefore, spiking deconvolution that shortens the length of the input pulse is first applied to Temrez 3D seismic data, in an attempt to sharpen reflections and increase vertical resolution.

Seismic reflection data often displays a ringing pattern that occurs due to the presence of reverberation energy caused by reflections from multiple interfaces known as multiples. Fortunately, arrival times of multiples can be predicted and removed by predictive (gapped) deconvolution that uses autocorrelation algorithm. In this study, the predictive deconvolution is applied to the Temrez 3D seismic data using an operator length of 256 milisec and various prediction gaps ranging between 8 and 48 milisec. The prediction gap of 24 millisec, minimized the present reverberation energy most efficiently and therefore is chosen for seismic data processing in this study.

For visual inspection, shot gathers after deconvolution are plotted in Figure 17.

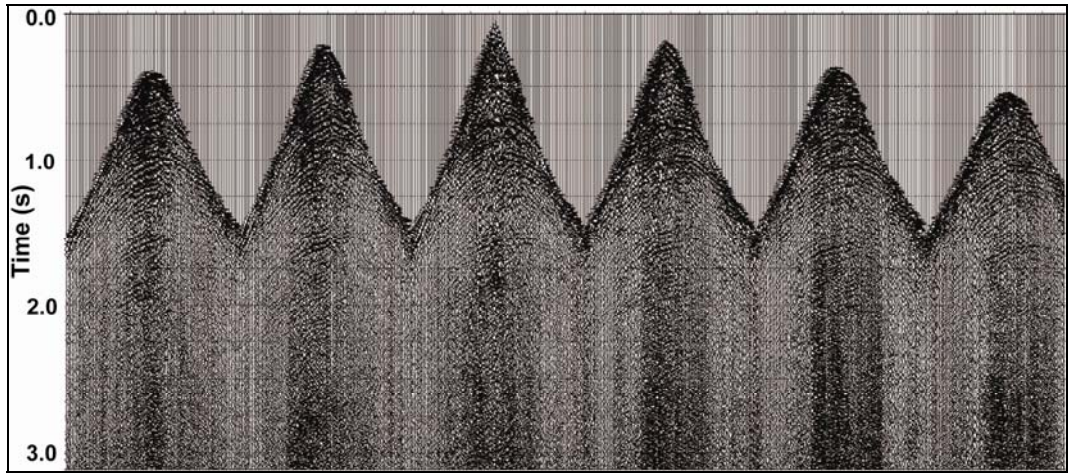


Figure 17: Shot gathers after deconvolution.

3.5 Gather

A collection of traces recorded from a single shot, which are stored in the database by the shot number, is called a shot gather. In shot gathers, each reflection occurs at a different point on the interface. In the gather process, all seismic traces with the same reflection point (common mid-point), are sorted from the complete data set of shot gathers to form common mid-point (CMP) gathers (Figure 18).

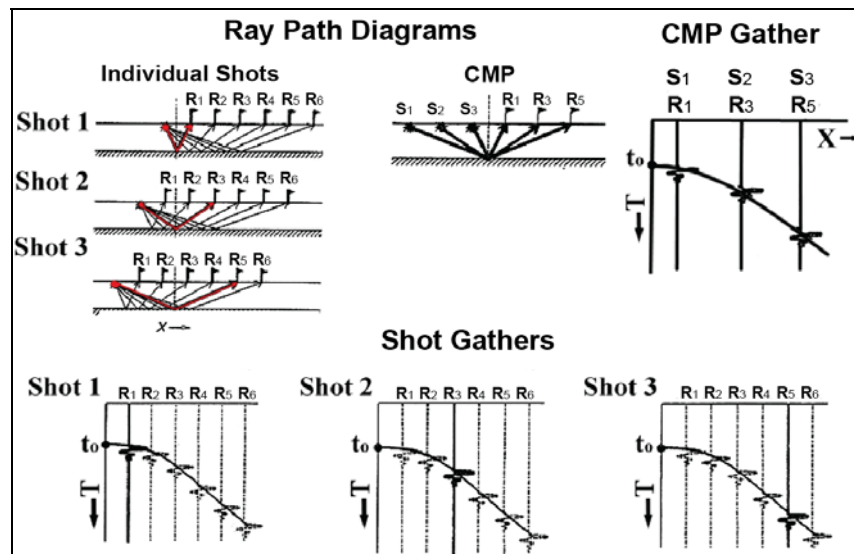


Figure 18: Simple illustrated example of common mid-point (CMP) gathering taken from Lillie (1999).

3.6 Static correction

The Earth has significant topography and the near-surface geology that can be highly variable, due to weathering and other effects. Both factors will cause the travel time of seismic waves to vary between traces. These delays are called statics because they lead to a shift in the arrival time of reflected waves in a seismic trace.

Application of large static shifts prior to velocity analysis and Normal Moveout corrections distorts the hyperbolic character of reflected events. This complication is more evident at shallow travel times where the distortion significantly affects velocity measurements. To minimize this distortion, the datum statics are decomposed into two time components, one that corrects the data to a floating datum and another, much larger component that corrects the data to a final datum (Figure 19a). In this study, the static correction for floating datum is applied at every 40 CMP (1000 m) prior to velocity analysis and Normal Moveout corrections (Figure 19b), and the static correction for the final datum is reserved for post Normal Moveout correction.

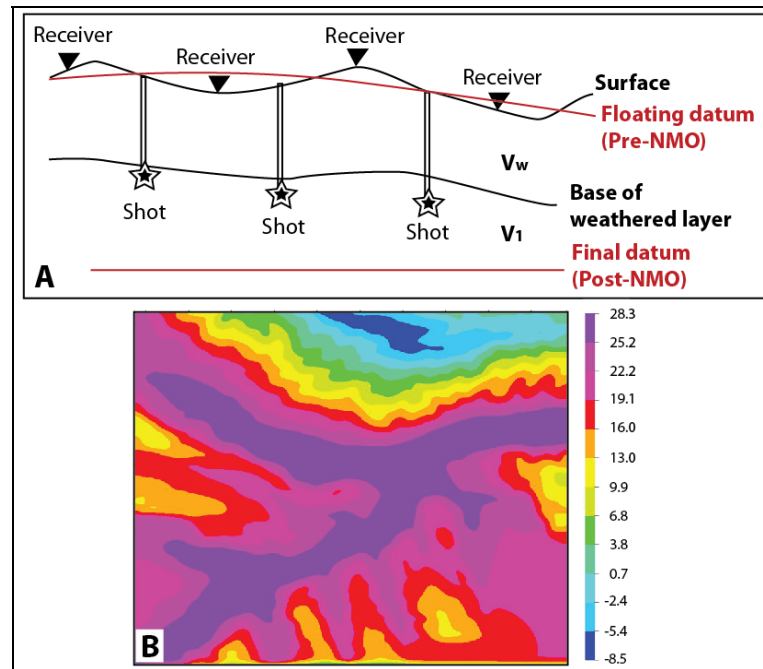


Figure 19: a) Datum statics terminology. b) Floating datum statics of the study area.

3.7 Velocity analysis

Reflections appear as hyperbolic events on the shot or CMP gathers. The arrival times of a reflected wave depends on distance where seismic energy travels. To make hyperbolic event flatten the appropriate velocity for individual CMP was chosen (known as Normal Moveout Correction). Normal Moveout (NMO) corrections are computed for narrow time windows down the entire trace, and for a range of velocities, to produce a velocity spectrum. The suitability of each velocity value is assessed by calculating a form of multi-trace correlation, the semblance, between the corrected traces of the CMP gather, which assesses the power of the stacked reflections. Then, a velocity function is derived by picking the location of the peaks on the velocity spectrum plot.

Velocity analysis in this project consists of two stages, initial and final velocity analyses. Initial velocity analysis is performed to the seismic data at analyzing points that separated by 1200 m along the crosslines and inlines. Each analyzing point is composed of 40 CDP with length 500 m. Picked velocities at each CDP are stored into the Paradigm Focus database as velocity function. This velocity function is used to apply NMO-I correction to the seismic data. As it mentioned before, static correction for floating datum is calculated and applied after initial velocity analysis, than resultant seismic data was used as an input to final velocity analysis. In the final velocity analysis interval between analyzing points was decreased to 600 m, and 24 CDP with length 300 m on each point (Figure 20). The final velocity function was used to apply NMO-II correction to the seismic data. Static correction for floating datum is calculated and applied second time after final velocity analysis. Finally, the seismic data was muted and stacked in to the brutestack-4 (Figure 21).

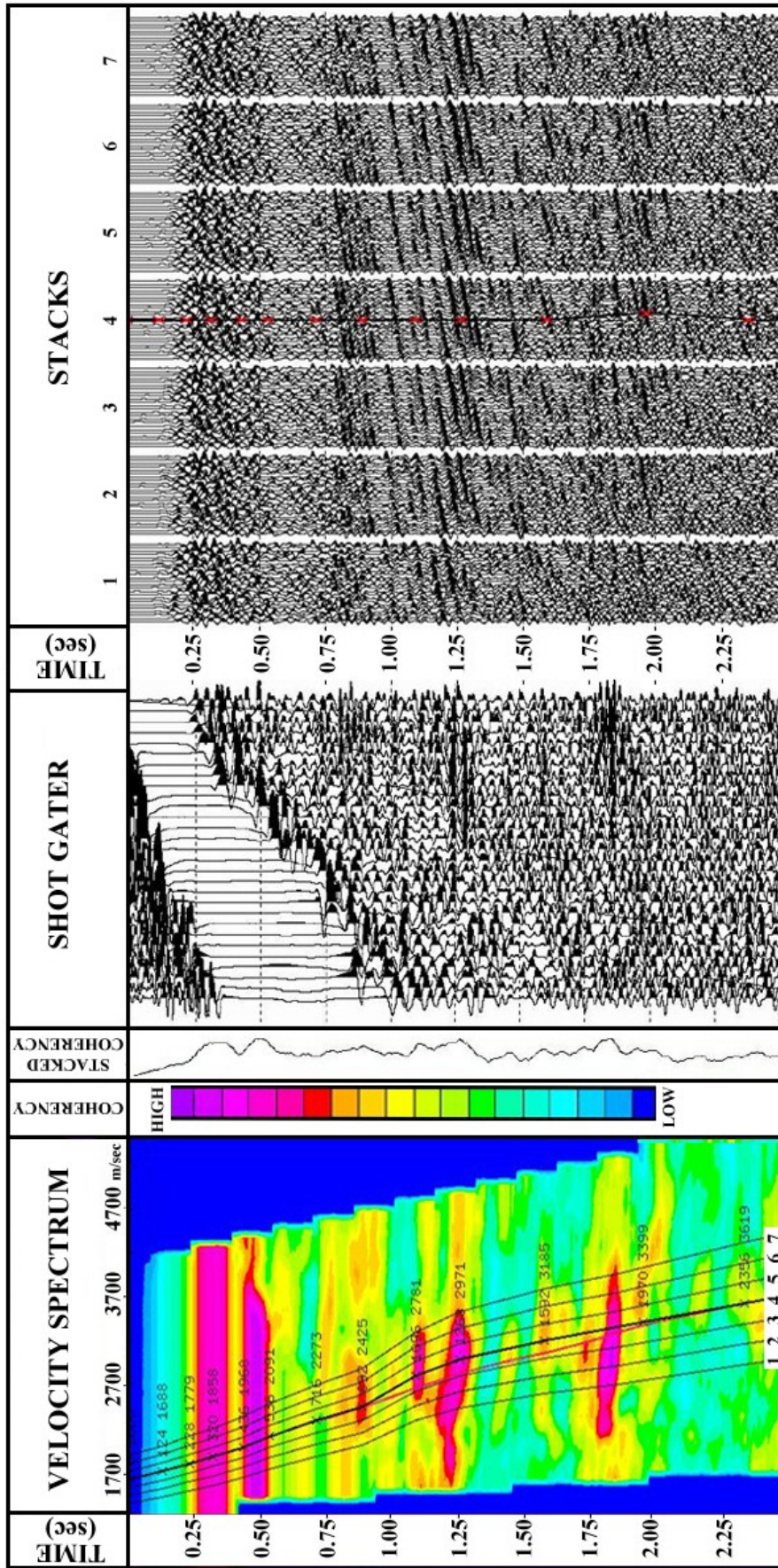


Figure 20: Results of the velocity analysis and normal moveout (NMO) correction (velocity spectrum, shot gather and stacks) conducted using updated residual statics. Note that the picked NMO corrected stacking velocity function (4) is shown in bold.

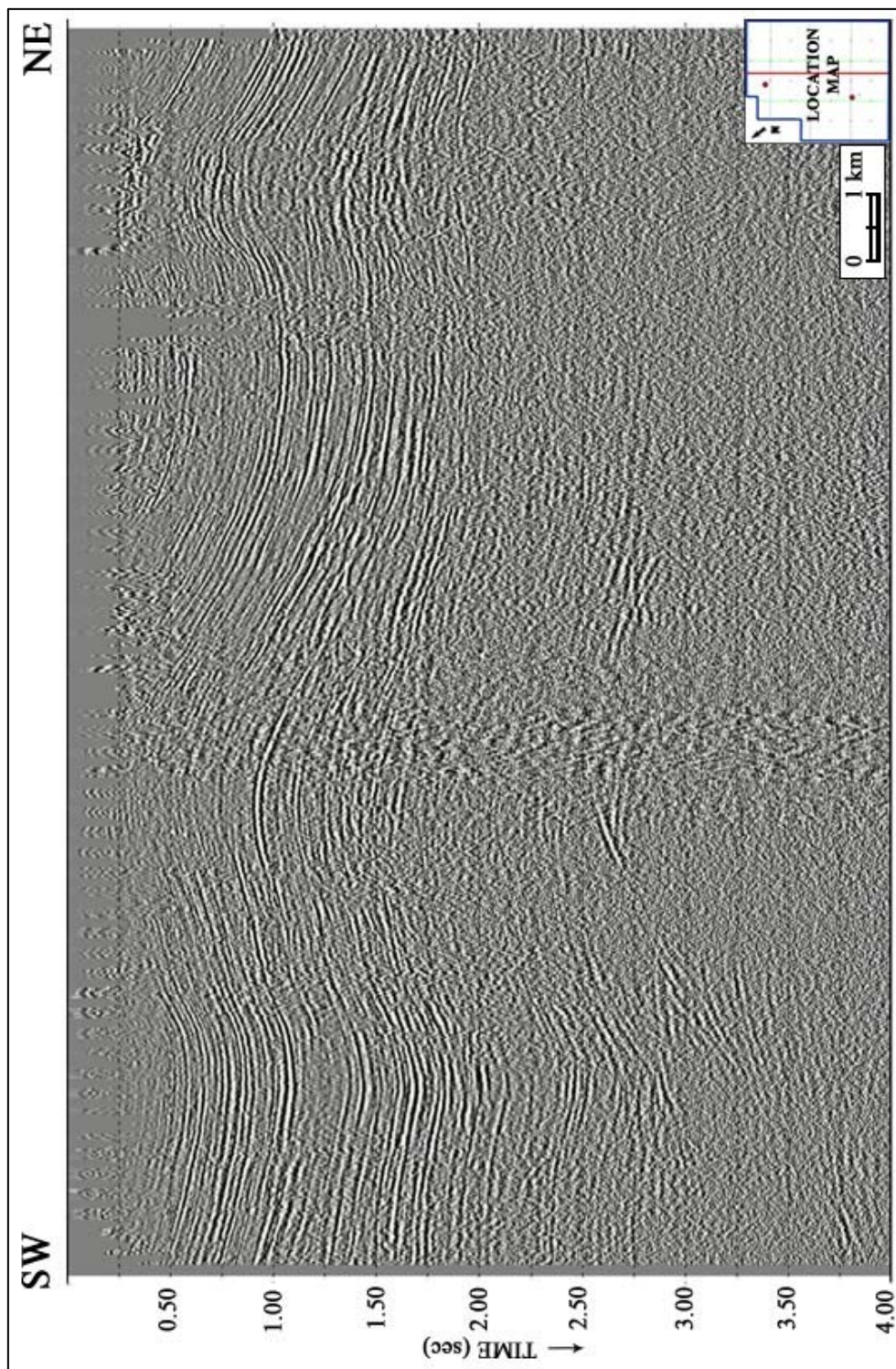


Figure 21: Seismic cross-section (crossline no: 2262) of stacked data after normal moveout (NMO) correction. Location of the cross section is shown in inset map along with boreholes.

3.8 Dip Move-Out (DMO) Correction

For dipping reflections, the traces of a CMP gather do not involve a common reflection point and therefore the stacking velocity depends on the dip of the reflector. The dip moveout (DMO) correction compensates for the dip effect in the NMO equation and effectively corrects for the reflection-point smear that results when reflectors dip. In this respect, DMO correction improves the velocity analysis and provides DMO velocities that stack events with various dips properly.

In this study, DMO correction is applied to NMO corrected pre-stack data, which includes selected CMP gathers at every 600 meters. The DMO velocity spectrum is derived using final datum statics that maximize the surface consistency by minimizing the effects of shot, receiver or surface conditions. New DMO corrected stacking velocities were then picked closer to shots to get consistent velocity fields and used to apply DMO correction to the entire seismic data set (Figure 22). For visual inspection, stacked cross-section after DMO correction is shown in Figure 23.

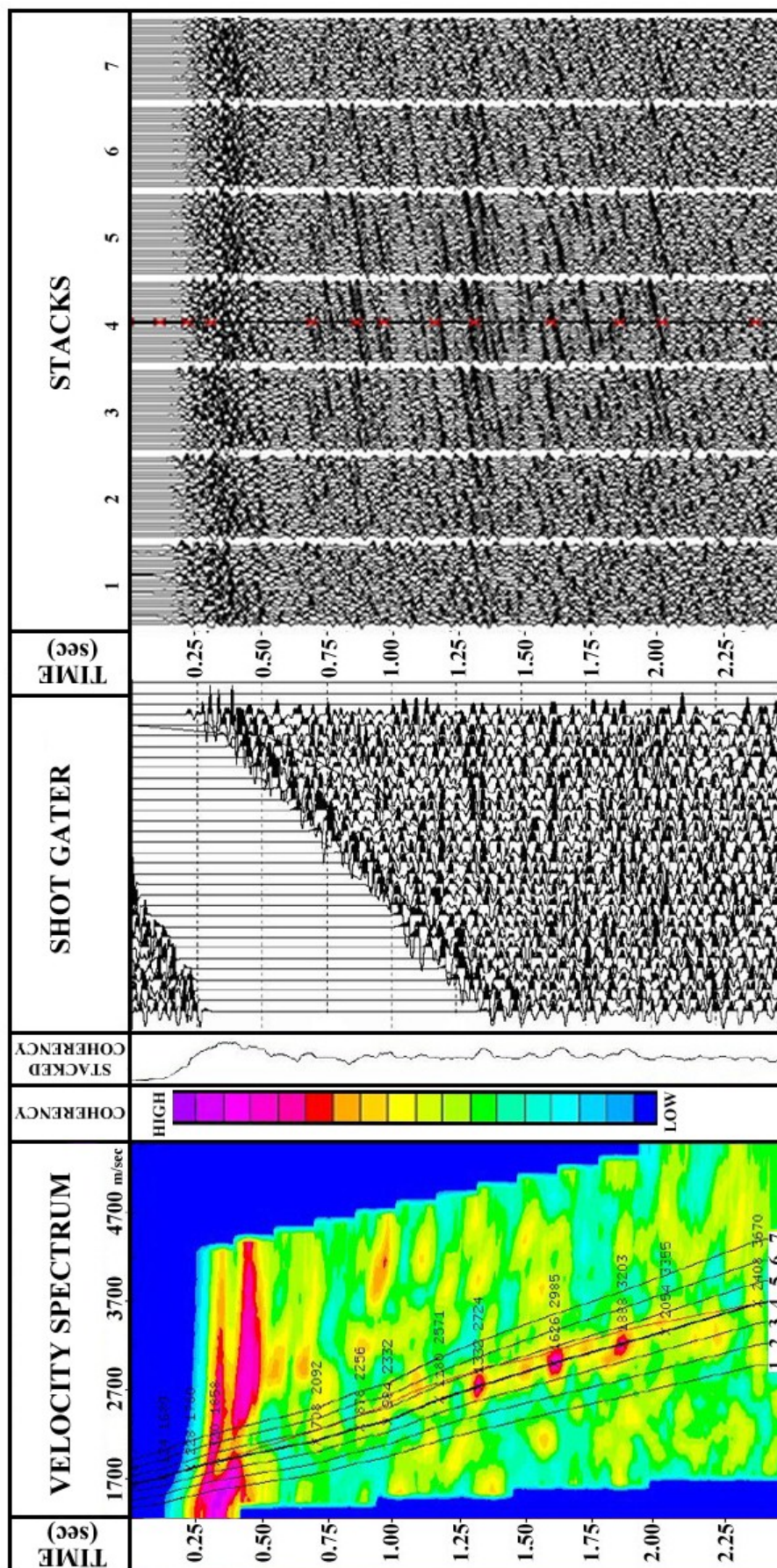


Figure 22: Results of the velocity analysis and dip moveout (DMO) correction (velocity spectrum, shot gather and stacks) conducted using final datum statics. Note that the picked DMO corrected stacking velocity function (4) is shown in bold.

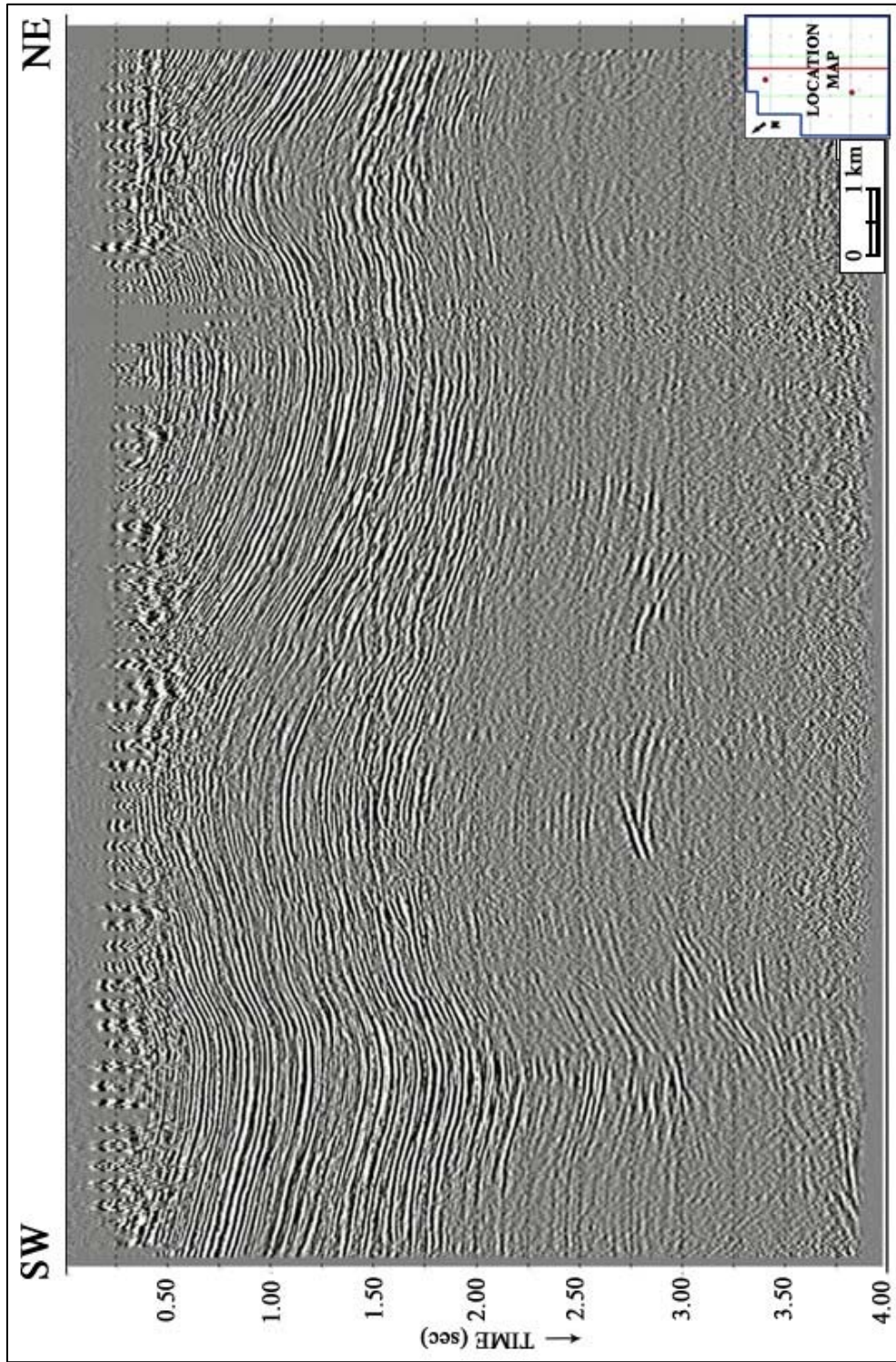


Figure 23: Seismic cross-section (crossline no: 2262) of stacked data after dip moveout (DMO) correction. Location of the cross section is shown in inset map along with boreholes.

3.9 Migration

In CMP gathers, it is assumed that the reflections of each trace occur directly beneath the midpoint of each gather. This is true only if the reflecting interfaces are horizontal. If the interfaces are dipping or if they are not planar, this assumption does not hold. The process of trying to move reflections back to their original position is called migration.

Pre-stack time migration, during which individual seismic traces in time domain are migrated before stacking, can remove the effect of offset on dipping events effectively producing a more coherent stack and therefore commonly used to image complex structures containing noticeable lateral velocity variations.

In this study, a Kirchhoff algorithm based on computation of the travel time surface from a source to a scatter point and summation of related energy (Schneider 1978), is applied to the pre-stack time migration (PSTM) of the Temrez 3D seismic data set.

Pre-stack Kirchhoff time migration relies on the construction of an accurate internal velocity model. During the construction of 3D velocity model, dip moveout corrected stacking velocities are served as initial migration velocity field. After removing the used velocity function from resultant pre-stack time migrated gather, the migration velocity spectrum is derived to pick more accurate migration velocities (Figure 24). Finally, the pre-stack time migration is again performed using the derived migration velocities to the entire data set to obtain the pre-stack time migrated seismic images (Figure 25) and their resultant interval velocity models (Figure 26).

After re-processing, the quality of the Temrez 3D seismic data is improved and seismic reflectors on the cross sections and timeslices acquired strong and continuous character that is more suitable for seismic interpretation. For comparison, see Figures 27 and 28.

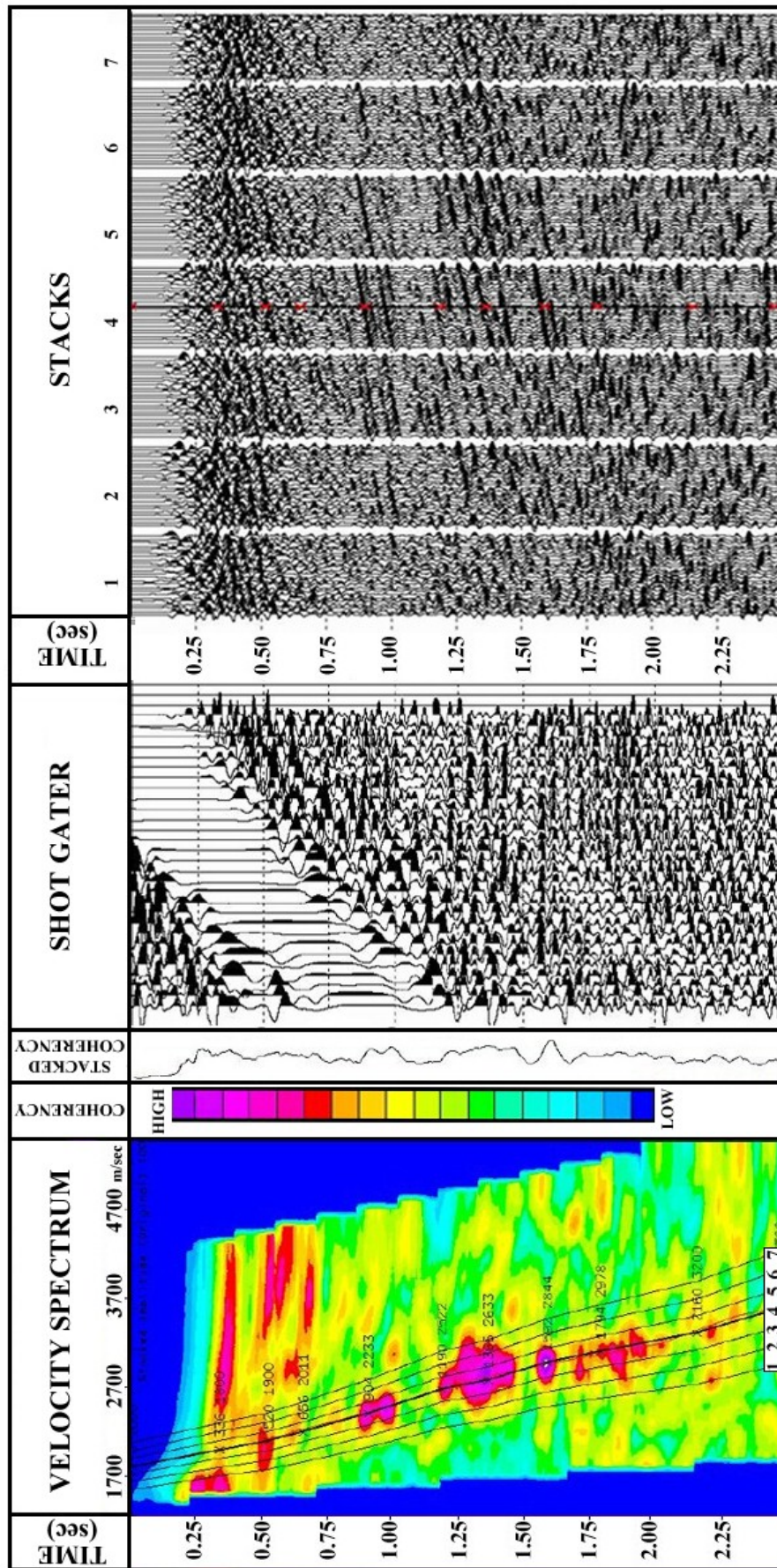


Figure 24: Results of the migration velocity analysis (velocity spectrum, shot gather and stacks) conducted. Note that the picked migration velocity function (4) is shown in bold.

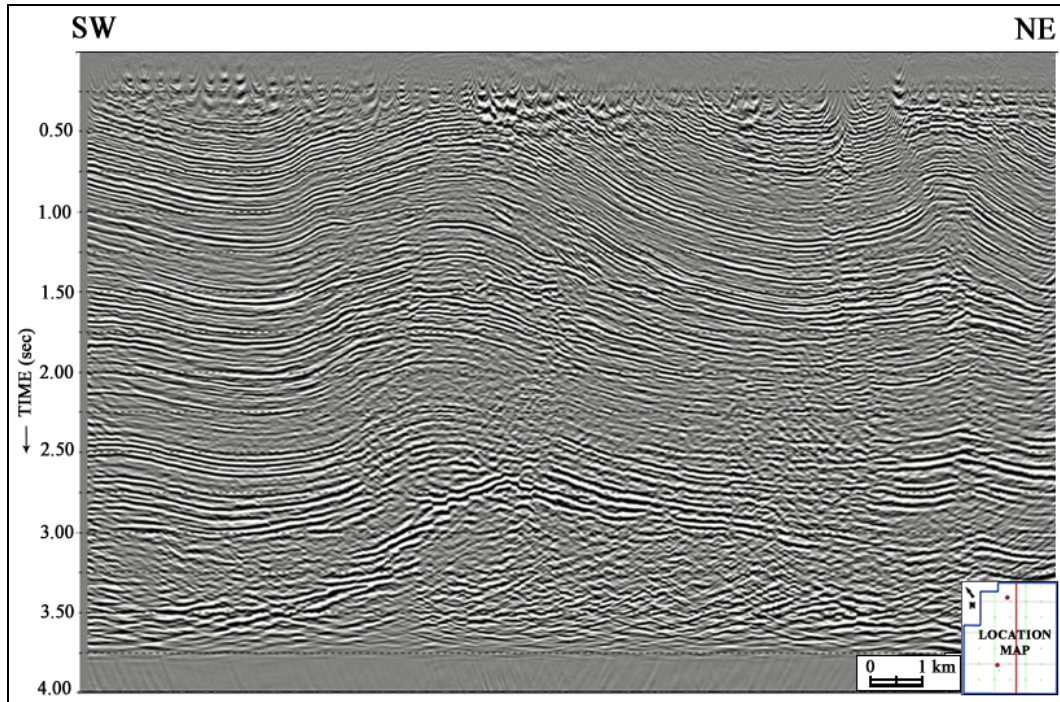


Figure 25: Seismic cross-section (crossline no: 2262) of stacked data after pre-stack time migration. Location of the cross section is shown in inset map along with boreholes.

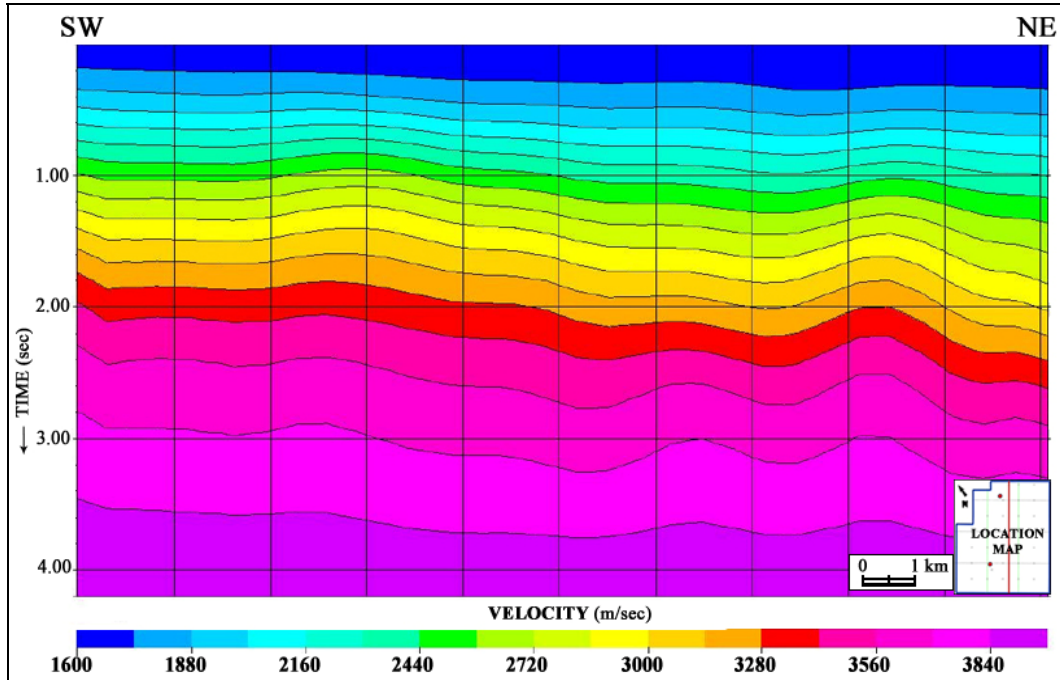


Figure 26: Interval velocity model of the seismic cross-section (crossline no: 2262). Location of the cross section is shown in inset map along with boreholes.

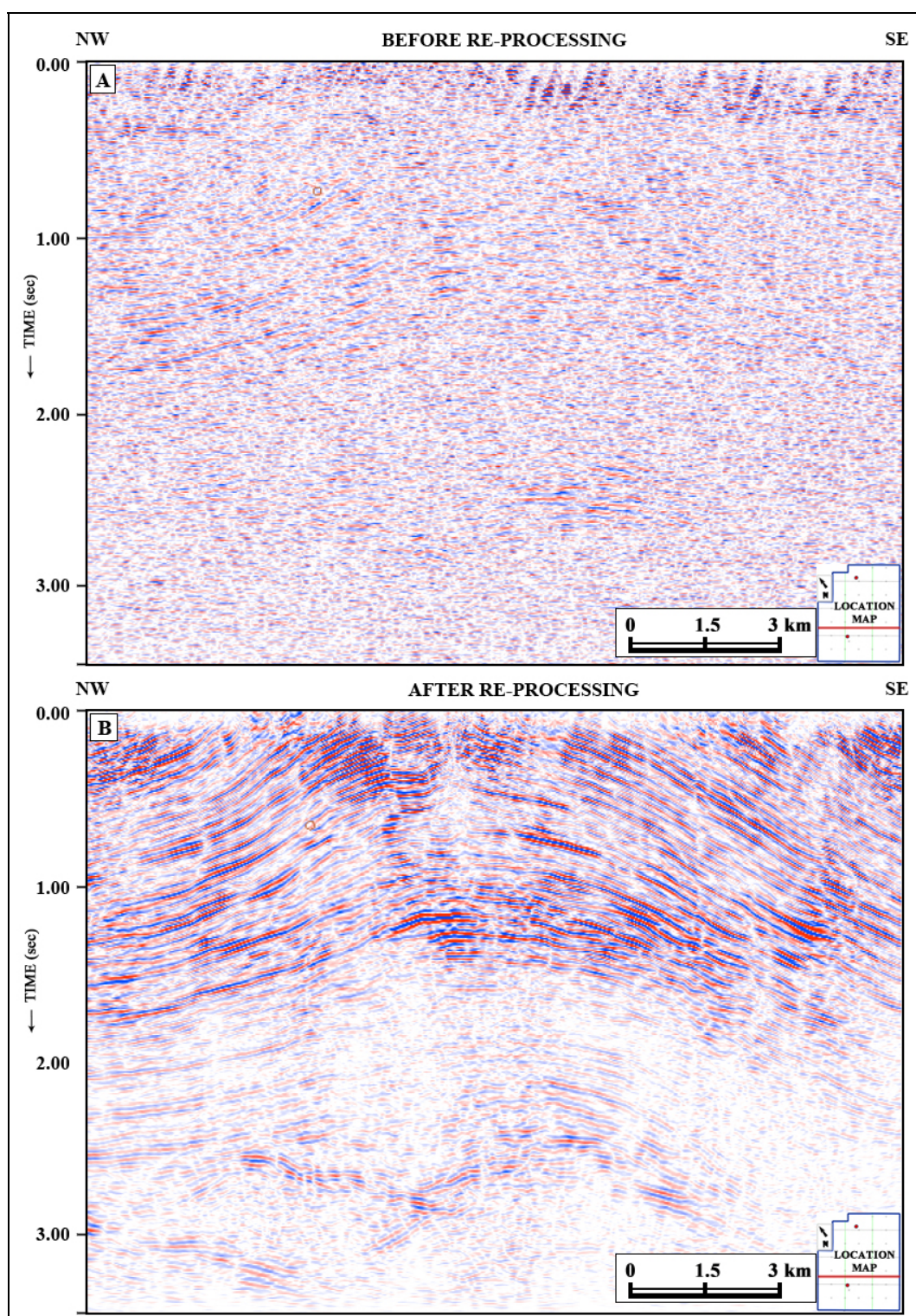


Figure 27: Seismic cross-sections (inline no: 5257). **a)** Before re-processing; **b)** after re-processing. Location of the cross section is shown in inset map along with boreholes.

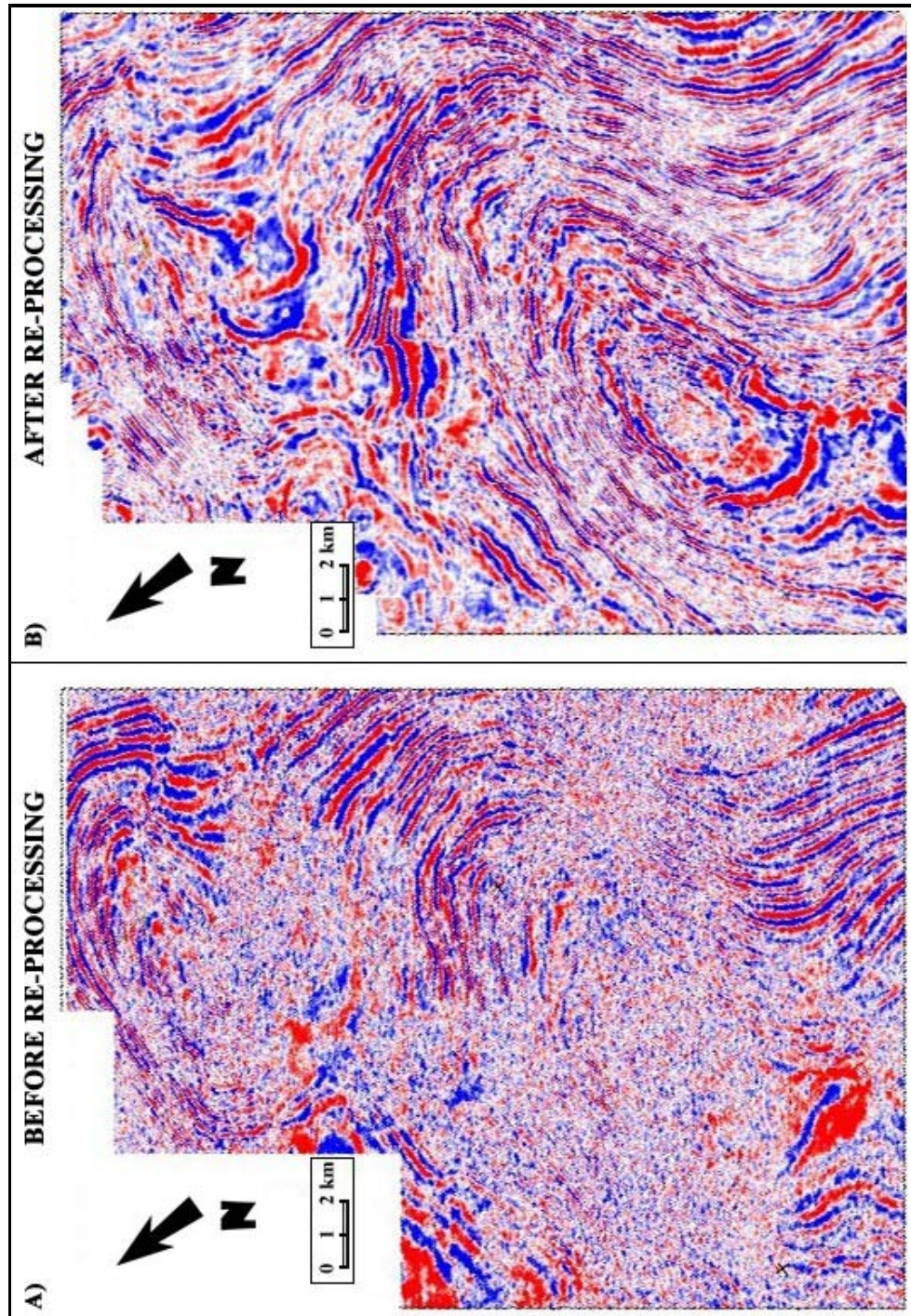


Figure 28: Seismic timeslices at 0.5 sec. **a)** Before re-processing; **b)** after re-processing.

CHAPTER 4

SEISMIC INTERPRETATION

4.1 Well-to-Seismic Tying and Horizon picking

Before horizon picking procedure the borehole data, which include information about locations of the wells, formation tops, log tables and time-depth charts, must be loaded into the seismic survey. Then target horizons can be picked.

For horizon picking two boreholes within and one borehole outside the study area are used (Figure 29). The boreholes inside the study area include Karakavak-1, Pancarkoy-1. The Karakavak-1 is located in the south part of study area and comprises four formation tops, which are Danişmen, Osmancık, Mezardere and Ceylan formation tops. Similarly, Pancarkoy-1 comprises the same formation tops and is located in the northern part of the study area. These boreholes which are within the study area are not deep enough to transect the basement, thus, Kozpinar-1 borehole is used for picking the basement, although, it lies outside the study area. In order to tie the basement to the 3D seismics of the study area, a 2D seismic line connecting the borehole to the study area is used (inset Figure 29).

Both Miocene Ergene Formation and Pliocene Kırçasalılı Formation are derived from fluvial environment and displays similar seismic characteristics. Since, they are not differentiated in the boreholes; these units are grouped and interpreted together as Mio-Pliocene Ergene Group that unconformably overlies the Danişmen Formation. In this respect, the picked top of the Danişmen Formation is in fact corresponds to the base of the Ergene Group which is not clearly seen in the western most part of the survey area due to low quality of shallow part of the

seismic cube. However, in the northeast and southeast part of the study area where the thickness of Ergene Group increases, the base of this unit is interpretable (Figure 29, 30).

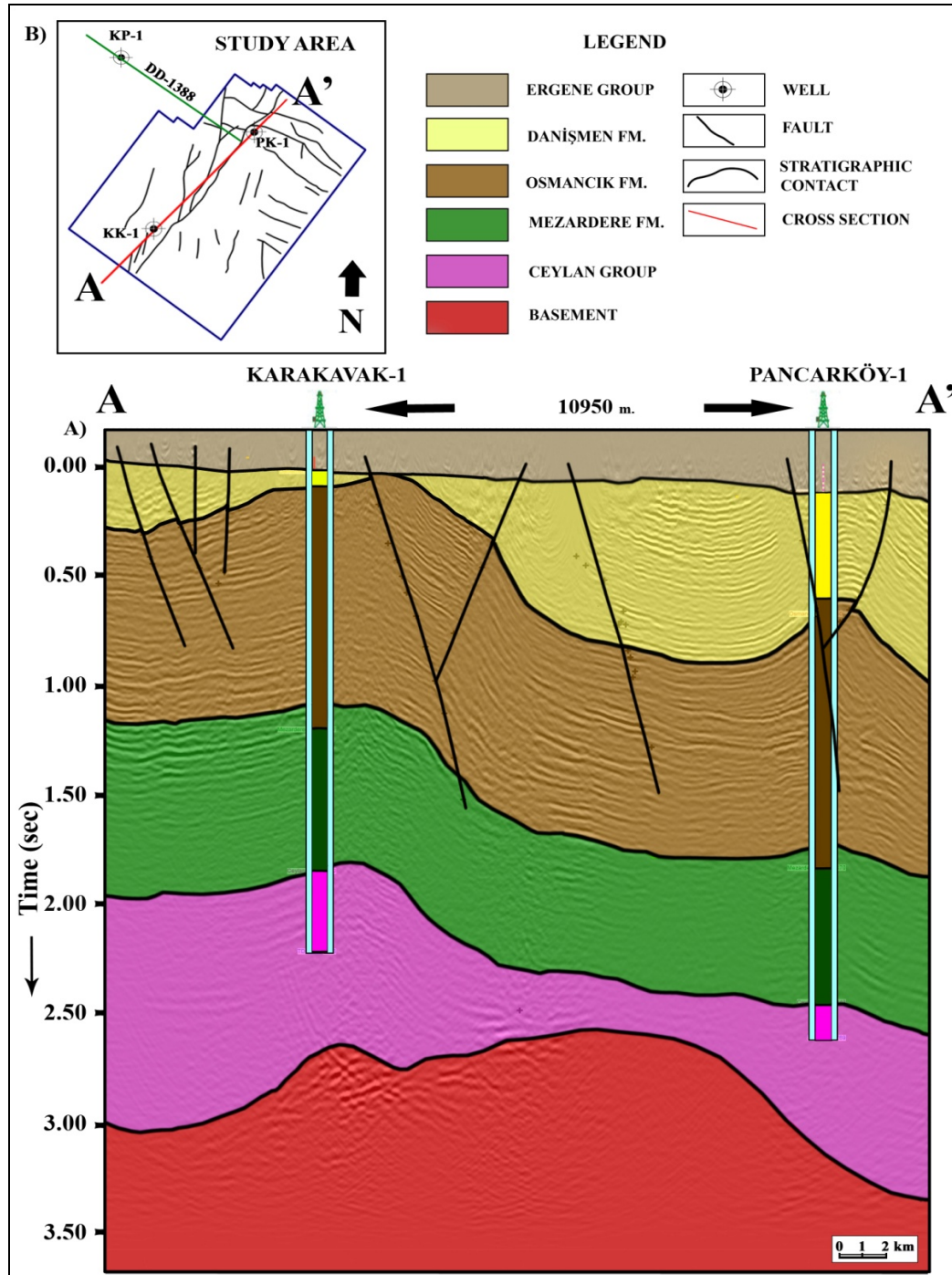


Figure 29: a) Seismic cross-section passing along the two boreholes located within the study area. b) Map of the study area showing the location of the cross-section, boreholes and 2D seismic line (no: DD-1388) used to tie the Kozpınar-1 well. KP-1: Kozpınar-1, PK-1: Pancarköy-1, KK-1: Karakavak-1.

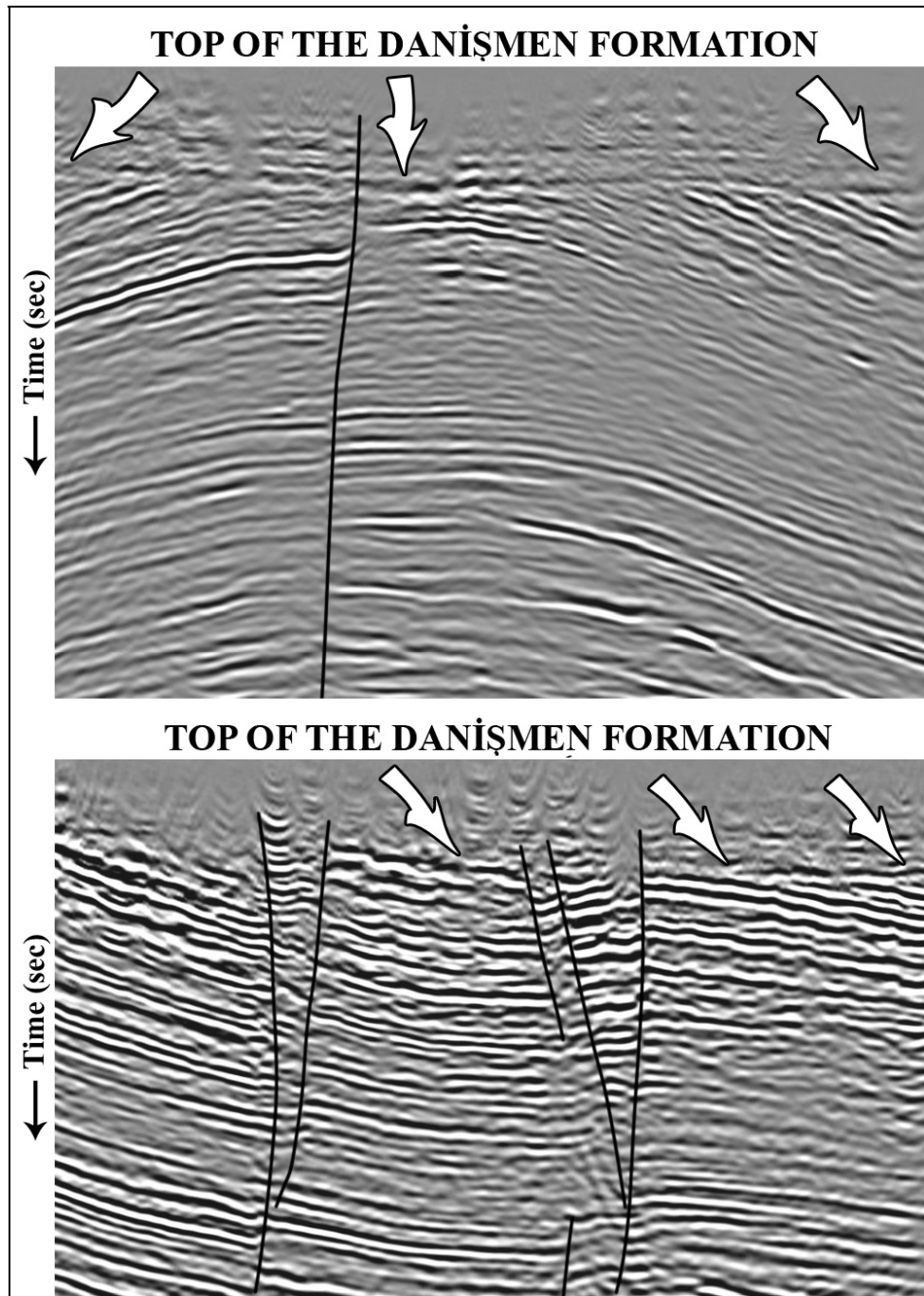


Figure 30: Seismic sections showing the unconformity surface at the top of the Danişmen formation.

The Danişmen Formation conformably overlies the Osmancik Formation and is of Late Oligocene in age. On the other hand, the Danişmen Formation shows thickness variation as such at the southern part of the study area the formation

thins down to tens of meters near the Karakavak-1 well while its thickness at the northern parts near the Pancarkoy-1 well, reaches as high as 700 m (Figure 29).

In this study, four horizons including top horizons of Osmancik, Mezardere, Ceylan formations and basement are picked in every 200 m interval for both in-line and cross-line directions throughout study area (Figure 31). Then, time differences of these interpreted units are mapped out to construct the isochron maps of the Osmancik, Mezardere formations and the Ceylan Group (Figure 32).

Osmancik Formation is Early to Late Oligocene in age and conformably overlain by the Danismen Formation. Its thickness is relatively uniform throughout the study area (Figure 31 and 32), although it decreases from 2000 at the Pancarkoy-1 well to 1767 m Karakavak-1 well.

Late Eocene-Early Oligocene age Mezardere Formation is conformably overlain by the Osmancik Formation and conformably overlies the Ceylan Group. Its thickness is relatively same throughout the study area (Figure 31 and 32) and it is 1433 m at Karakavak-1 and 1470 m at Pancarkoy-1.

The boreholes in the study area only cut down to Middle to Late Eocene Ceylan Formation. The Pancarkoy-1 well intersects the top of the Ceylan Formation at a depth of 4340 m and Karakavak-1 at 3320 m. Since, unstratified basement rocks at the bottom are characterized by discontinuous seismic reflections that can be easily distinguished from stratified units, the units between Mezardere Formation and basement are grouped and interpreted together as the Eocene age Ceylan Group, which conformably underlies the Mezardere formation and unconformably overlies the basement rocks. In the study area, the Ceylan Group show significant variations in thickness. In the center, the Ceylan group is relatively thick and becomes thinner towards north and south (Figure 31 and 32).

Upper boundary of the basement is picked using Kozpinar-1 borehole, which cuts the basement at the depth of 3289 m. Although, the location of the Kozpinar-1 borehole outside from the survey area, it is tied using a 2D seismic section that intersects both the Kozpinar-1 borehole and 3D Temrez seismic survey (Figure 29b). In the study area, top of the basement is shallower toward west (Figure 31).

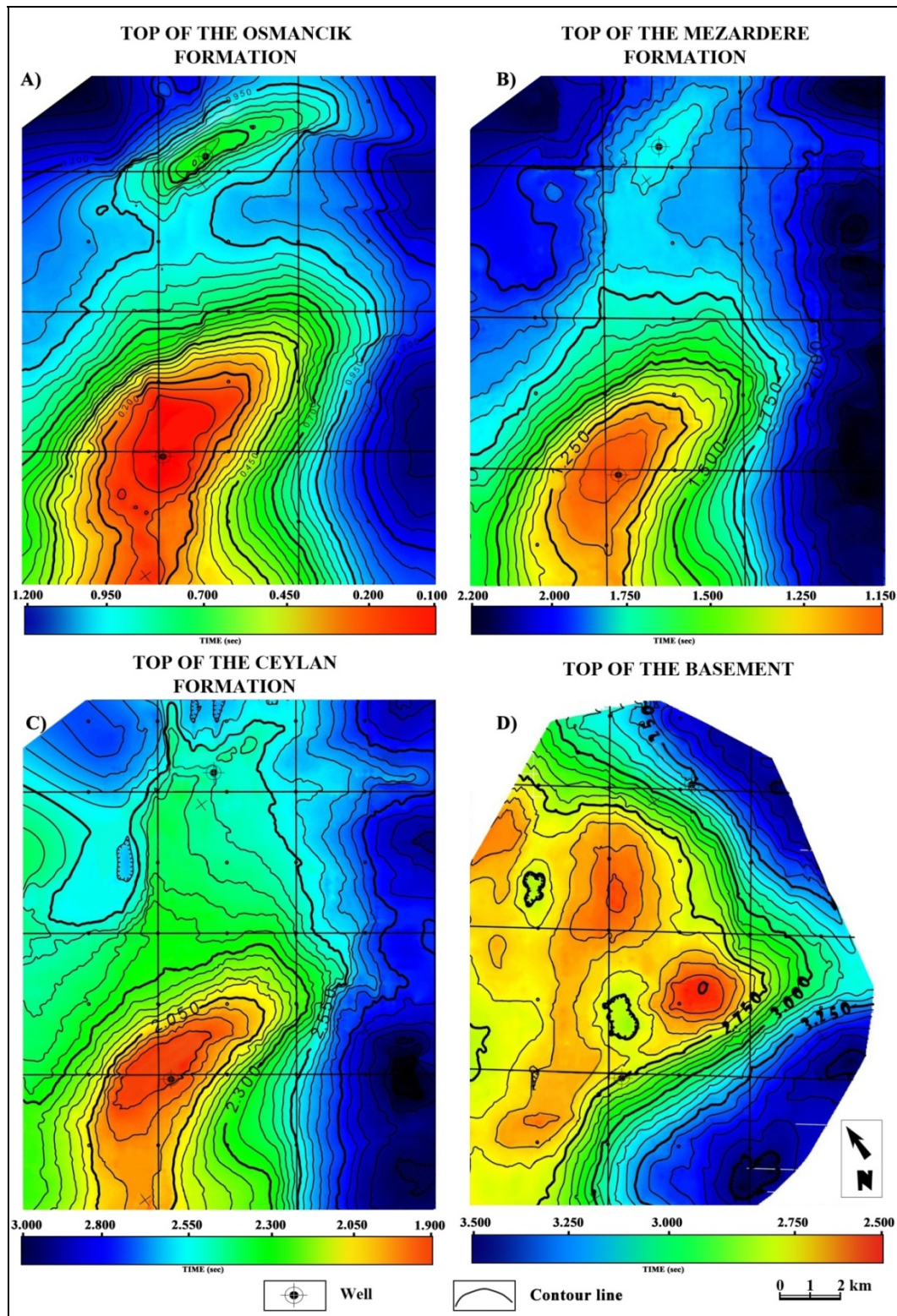


Figure 31: Color coded contour maps of the picked horizon tops of the formations in time domain.

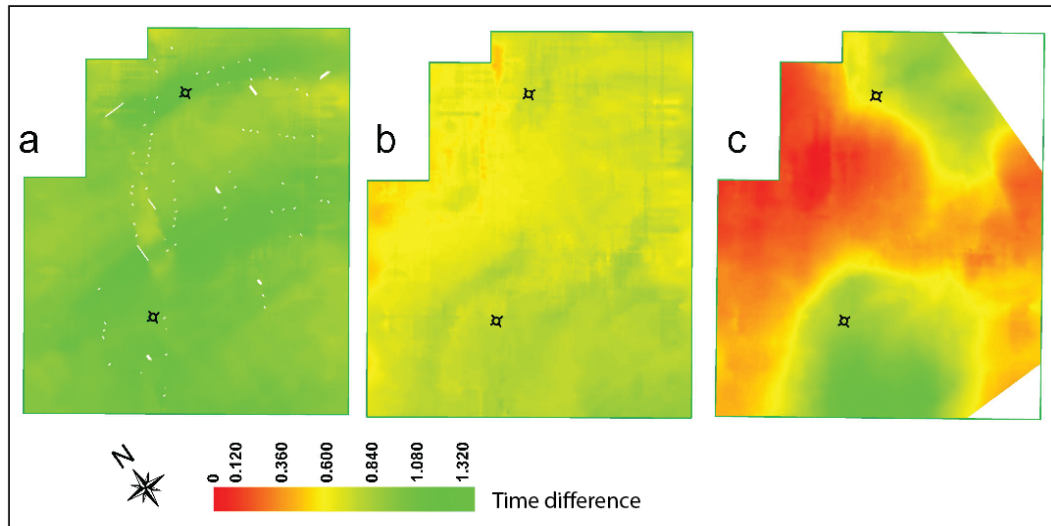


Figure 32: Color-coded isochron maps of **a)** Osmancık **b)** Mezardere formations and **c)** Ceylan group.

4.2 Folds

Two major doubly plunging anticlines are observed in the study area (Figure 33). One of the anticline is located in the northern parts of the study area has been reported previously as Babaeski High (Coskun, 2000). The second fold is recognized for the first time in this study and named as Karakavak anticline. The folded units include Oligocene Danişmen, Osmancık, Mezardere formations and Eocene Ceylan group. These folded units are overlain unconformably by unfolded Mio-Pliocene Ergene Group. Assuming there is no block rotation, observed folds suggest N-S directed compression during Miocene.

These folds are especially important for petroleum industry since they are the potential hydrocarbon traps. In this respect, Karakavak fold, which is identified first time in this study, can be an important target for future exploration efforts.

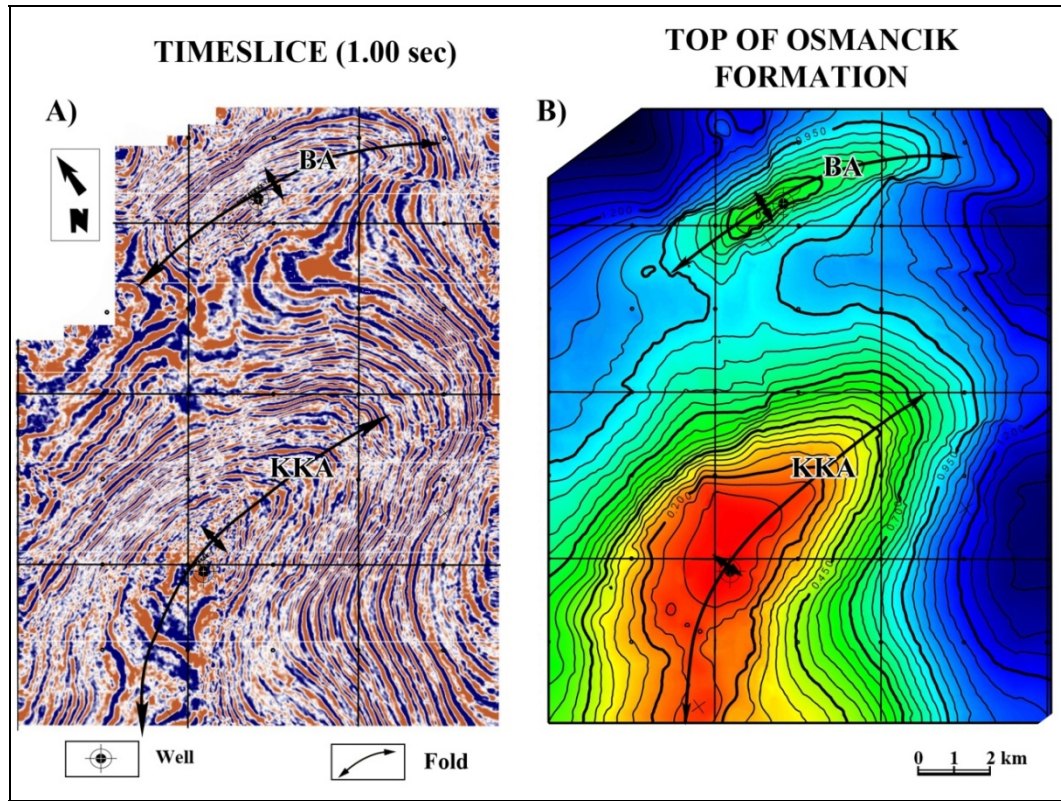


Figure 33: Doubly plunging anticlines observed in the study area. **a)** time slices at 1 sec, **b)** color coded time contour map of the top of Osmancık Formation. BA: Babaeski Anticline, KKA: Karakavak Anticline.

4.3 Fault Interpretation

In this study, faults are picked using sections with trace interval of 200 meters; however in the more complicated locations the trace interval decreased down to 50 m. During interpretation stage, only major faults that are long and continuous are included, the minor structures such as growth faults are omitted. Finally, fault offsets and cross cutting relationships are interpreted from both cross sections (Figure 34, 35, 36, 37 and 38) and time slices (Figure 39, 40, 41 and 42).

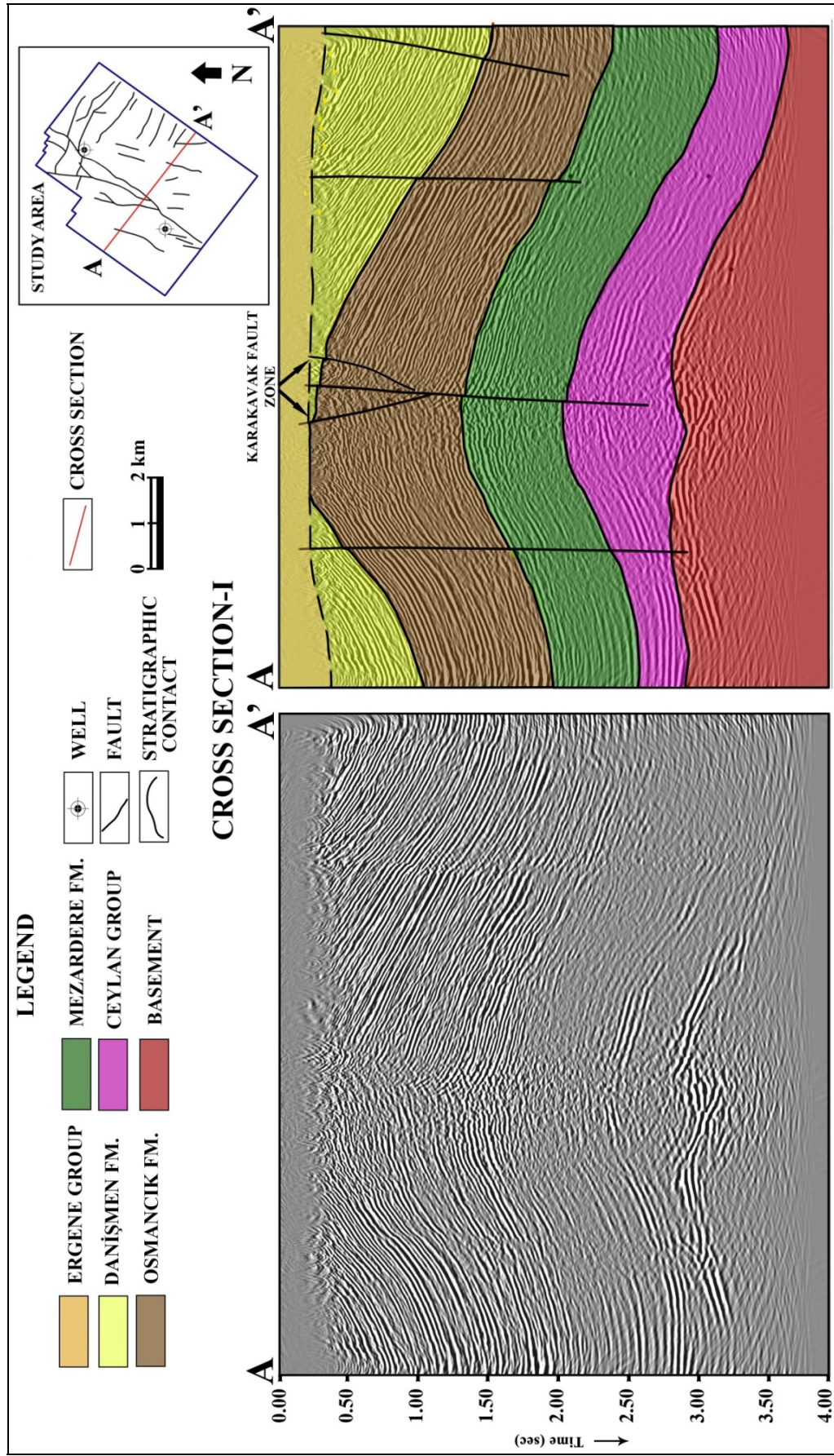


Figure 34: Raw and interpreted seismic cross-sections in time. Location of the cross-section is shown in the inset map along with boreholes and recognized faults.

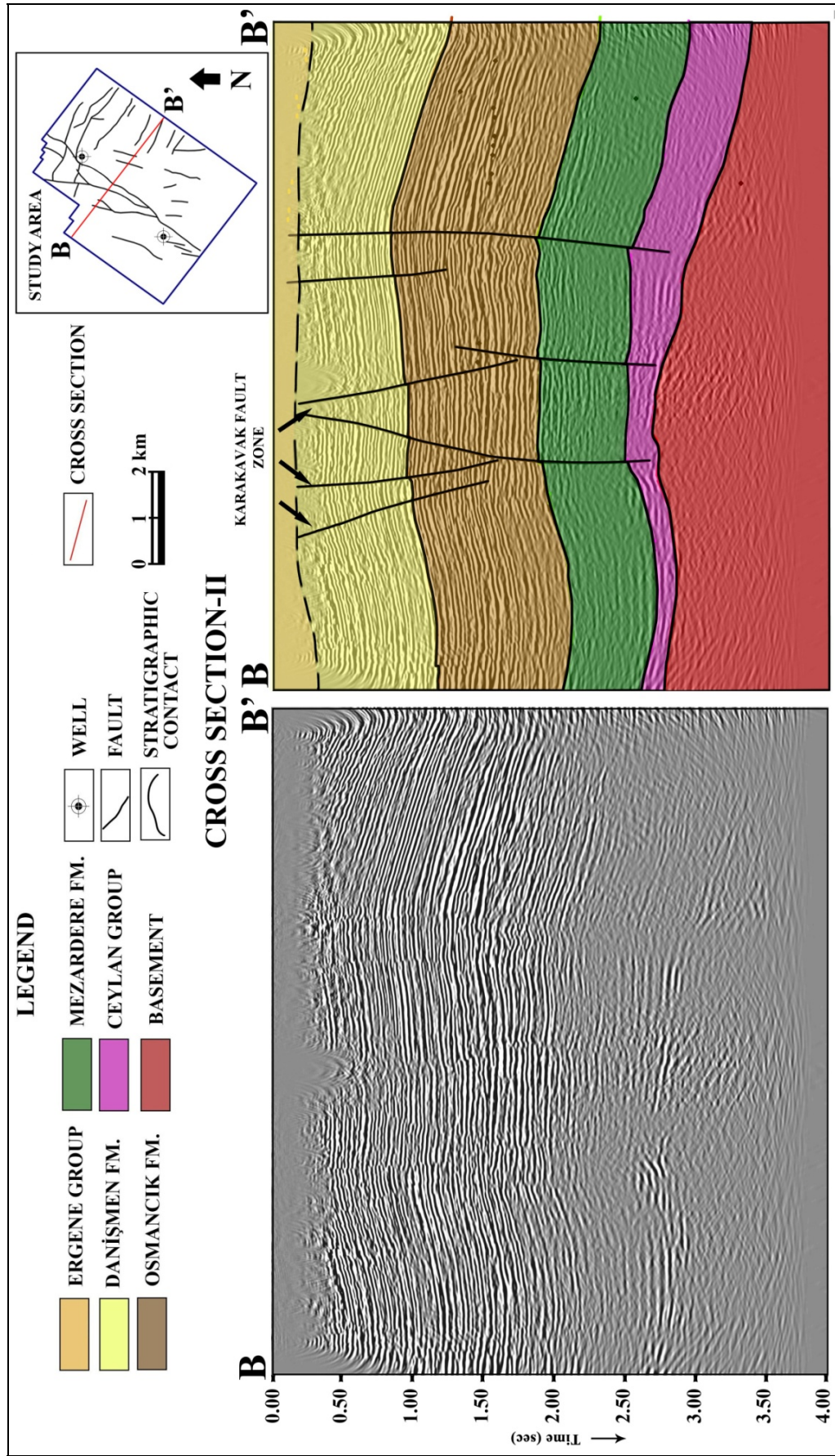


Figure 35: Raw and interpreted seismic cross-sections in time. Location of the cross-section is shown in the inset map along with boreholes and recognized faults.

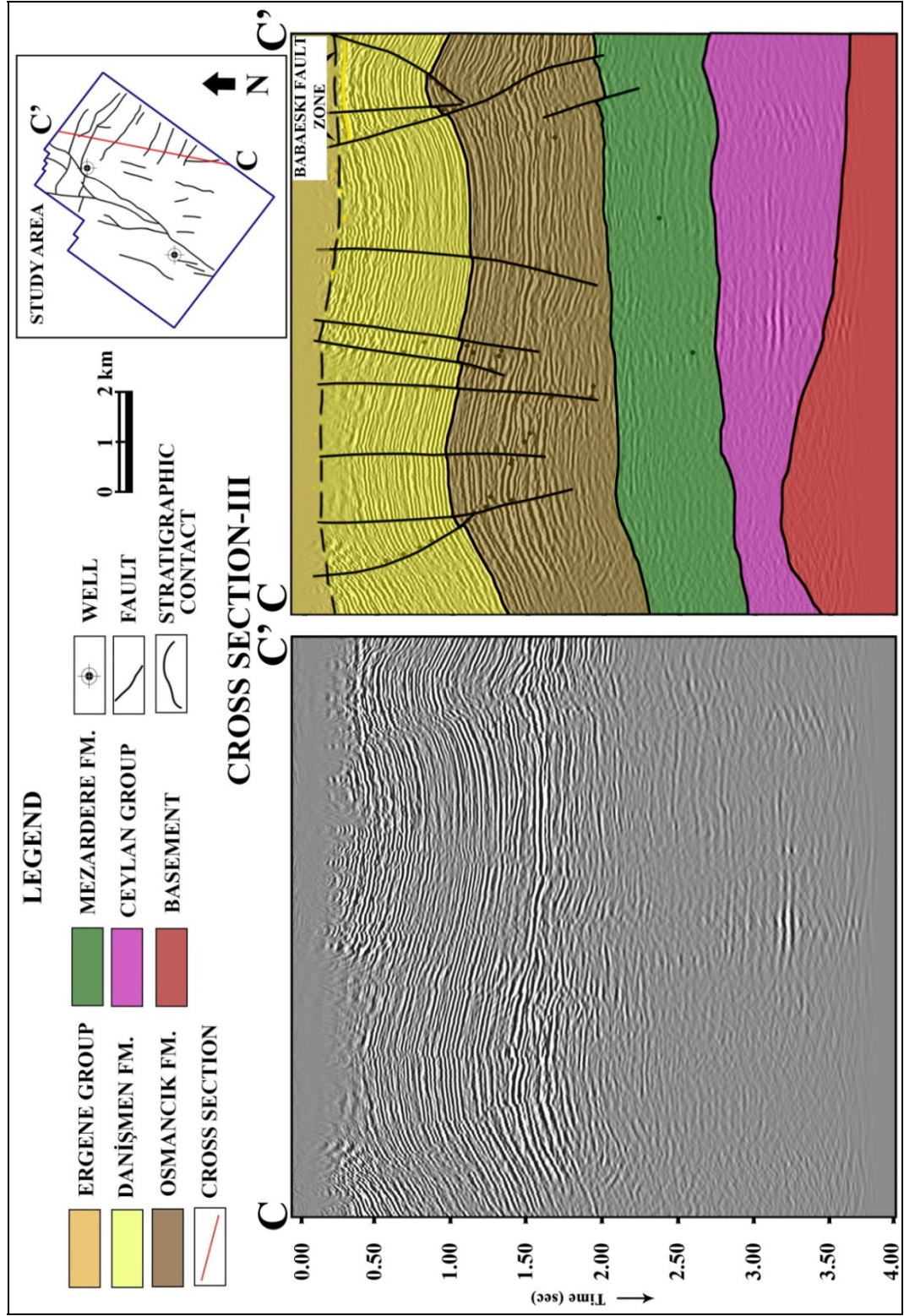


Figure 36: Raw and interpreted seismic cross-sections in time. Location of the cross-section is shown in the inset map along with boreholes and recognized faults.

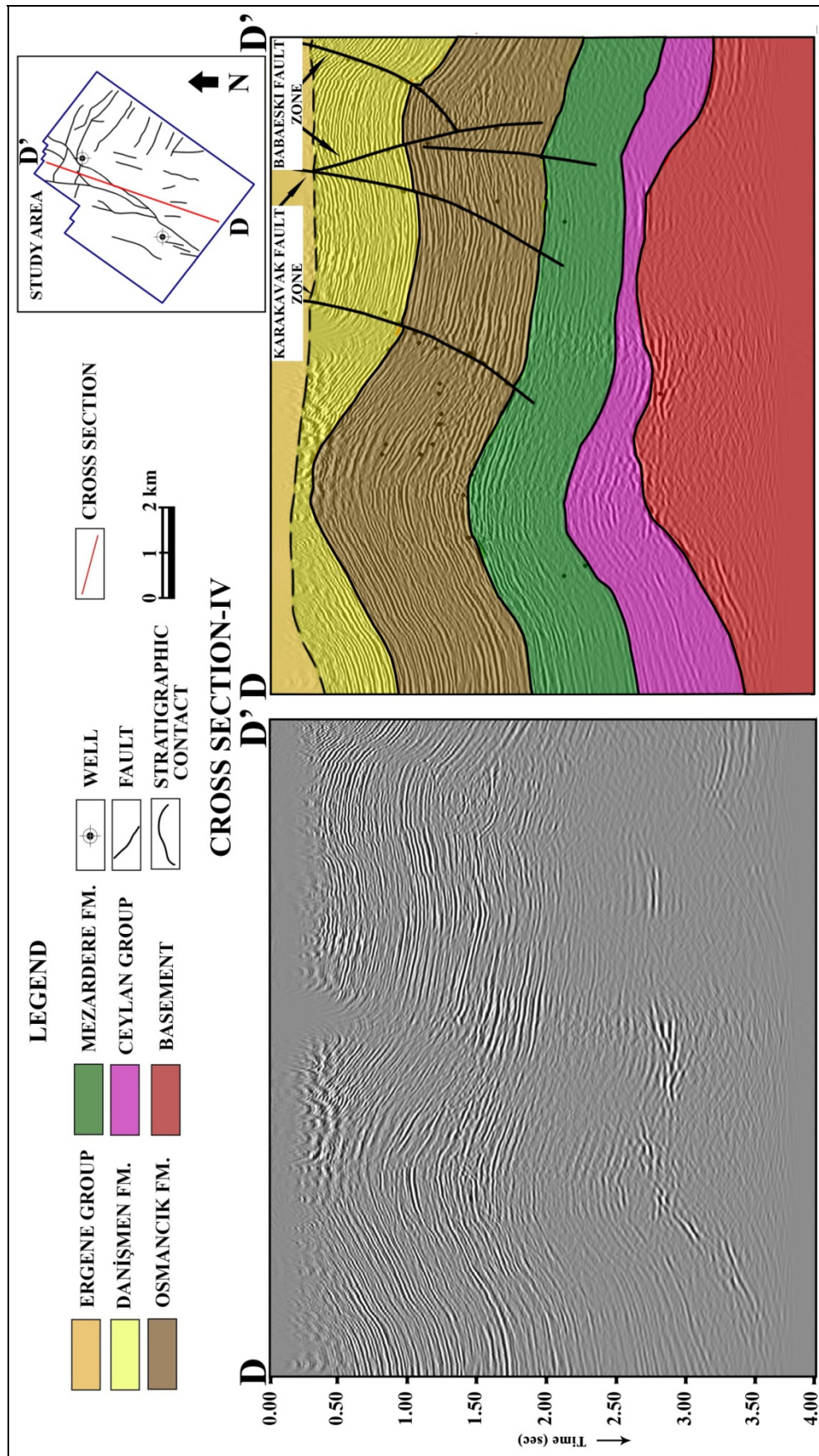


Figure 37: Raw and interpreted seismic cross-sections in time. Location of the cross-section is shown in the inset map along with boreholes and recognized faults.

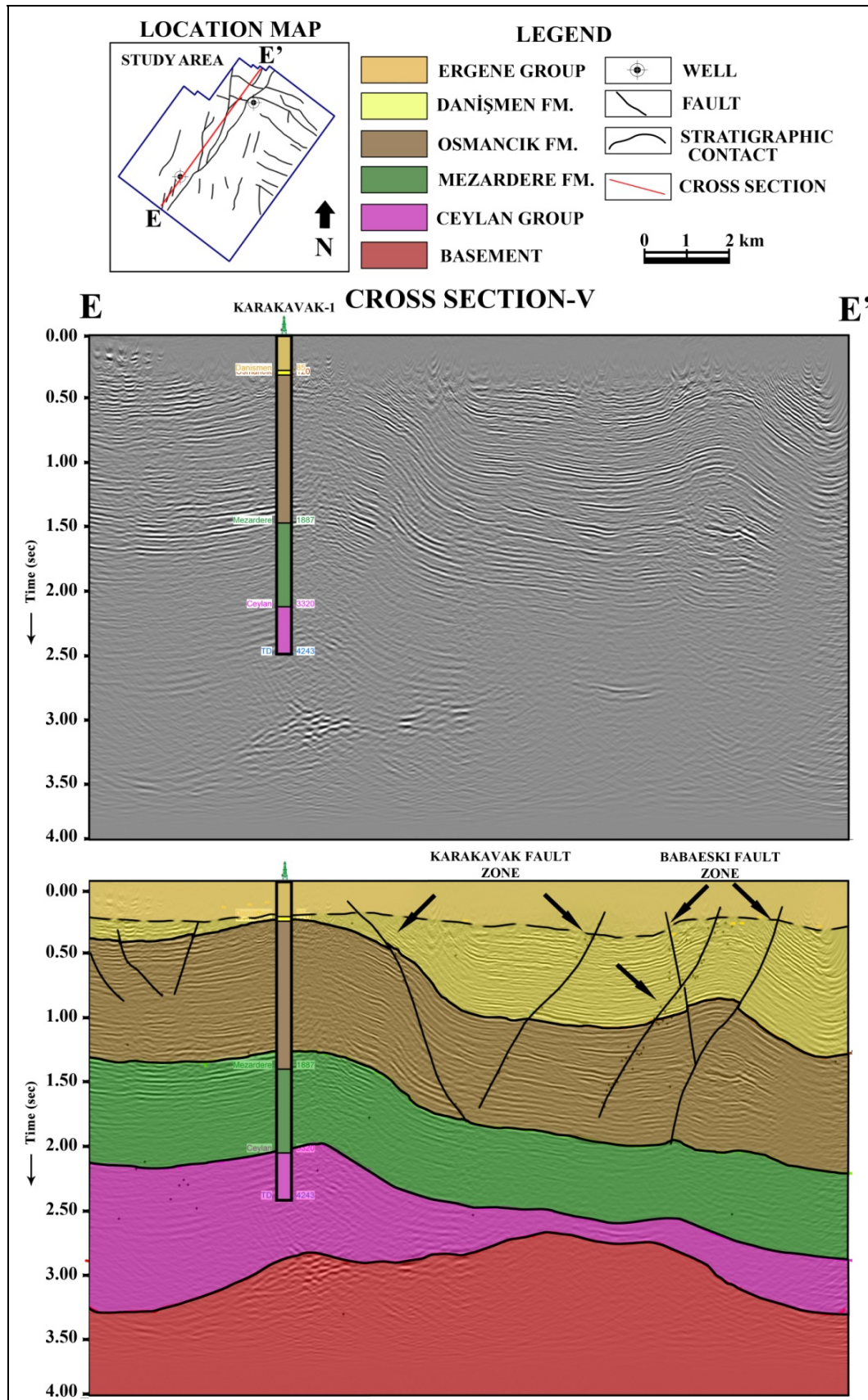


Figure 38: Raw and interpreted seismic cross-sections in time. Location of the cross-section is shown in the inset map along with boreholes and recognized faults.

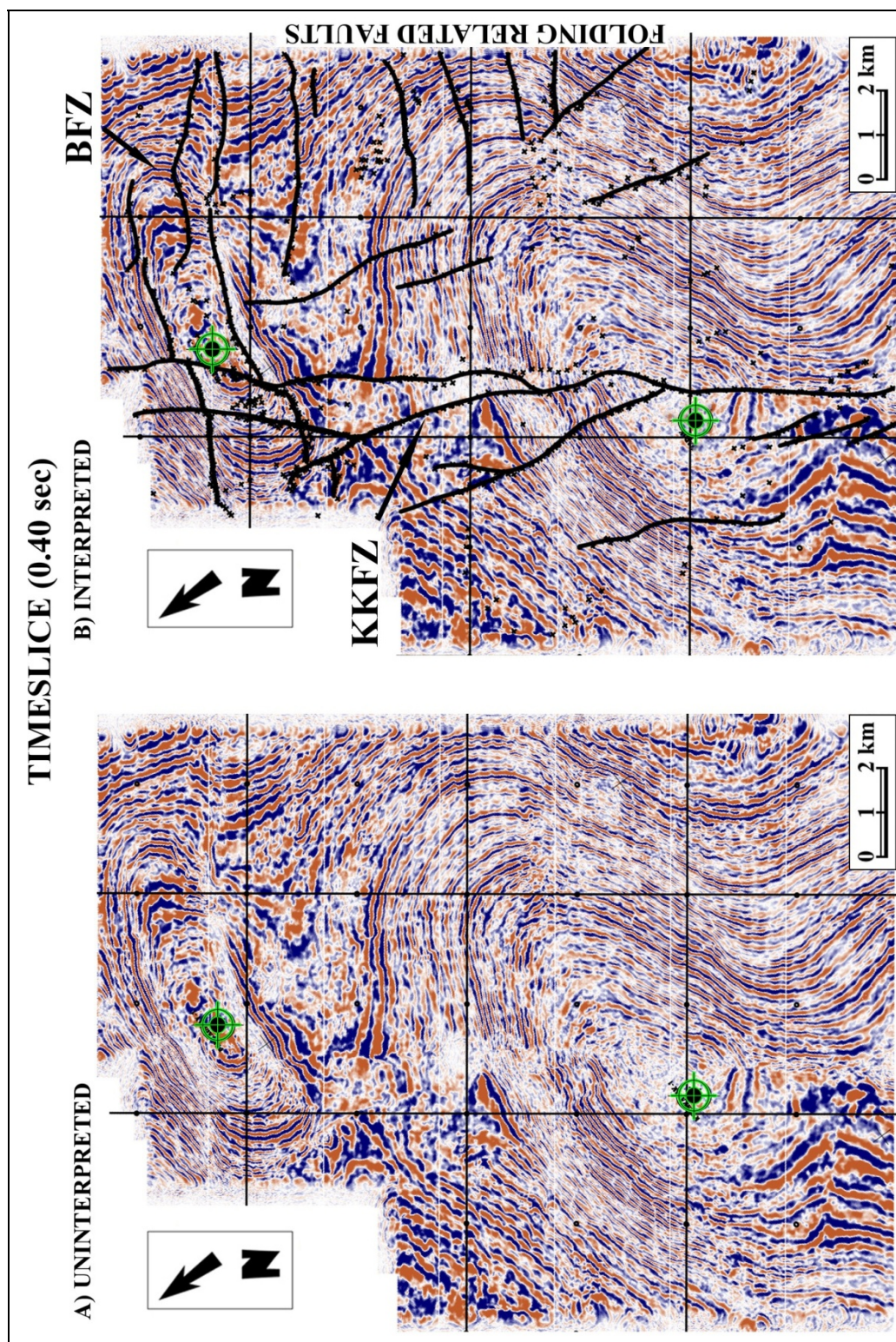


Figure 39: Raw (a) and interpreted (b) seismic time slices at 0.4 sec. BFZ: Babaeski Fault Zone, KKFZ: Karakavak Fault Zone.

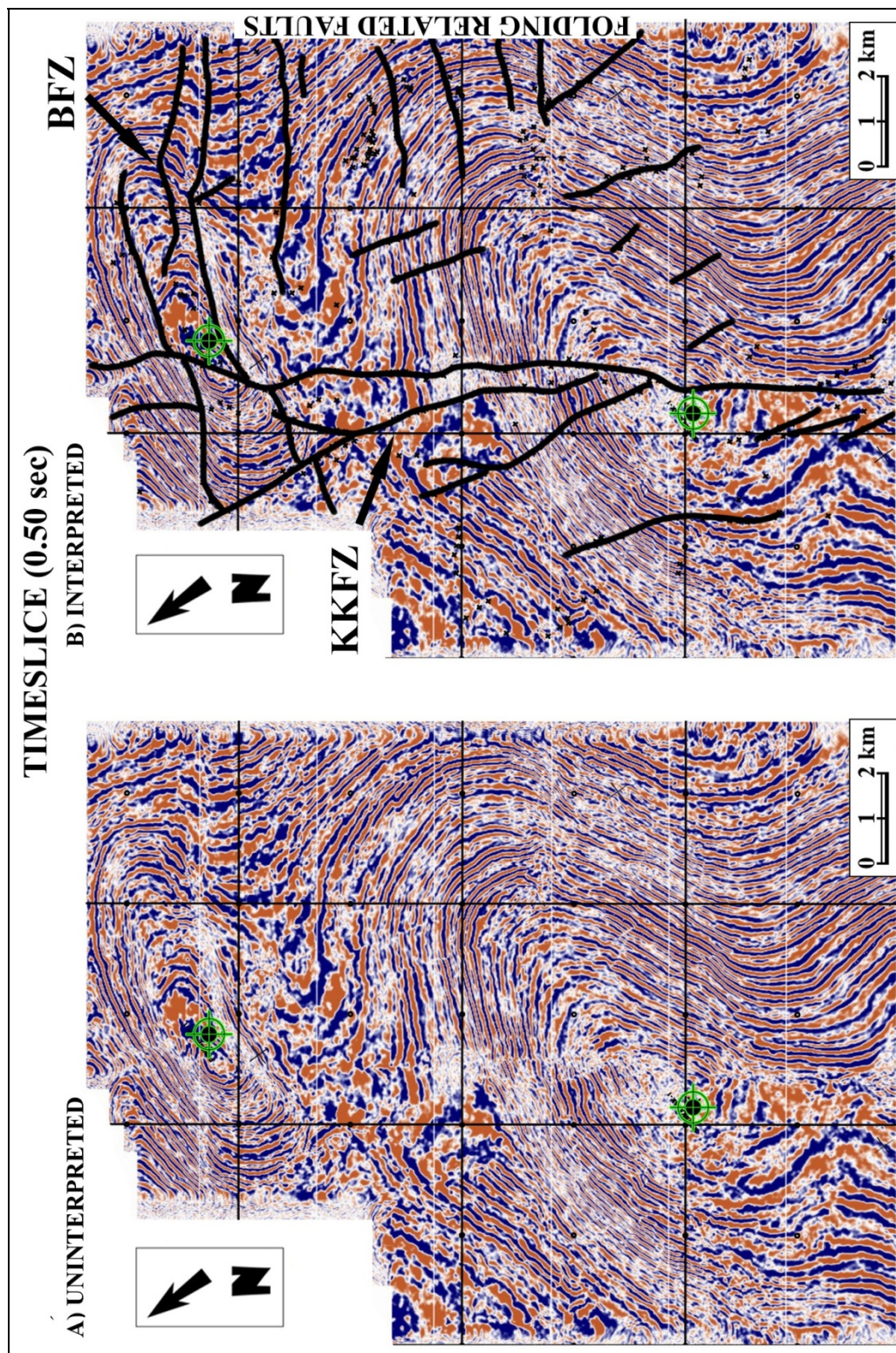


Figure 40: Raw (a) and interpreted (b) seismic time slices at 0.5 sec. BFZ: Babaeski Fault Zone, KKFZ: Karakavak Fault Zone.

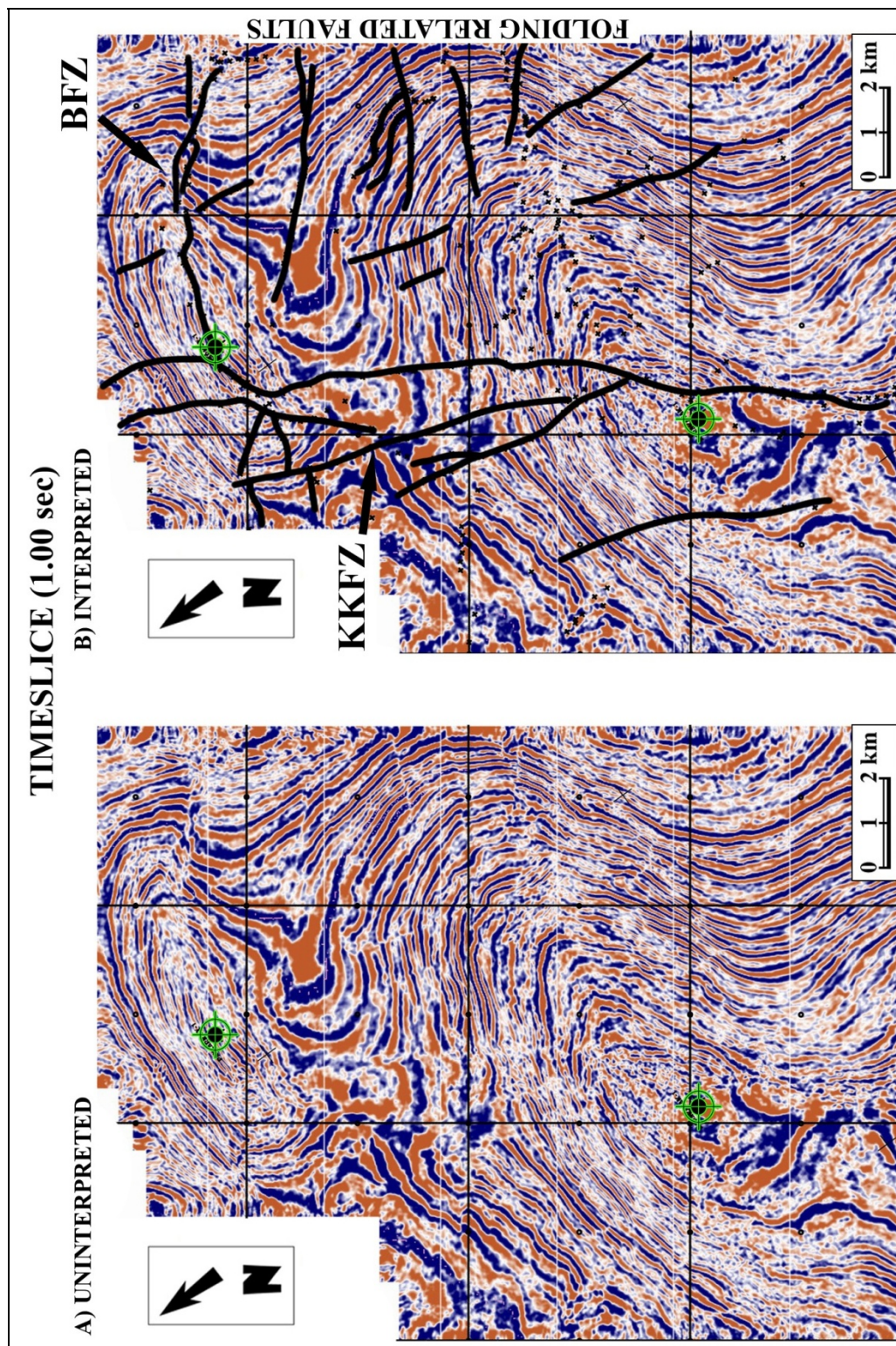


Figure 41: Raw (a) and interpreted (b) seismic time slices at 1.0 sec. BFZ: Babaeski Fault Zone, KKFZ: Karakavak Fault Zone.

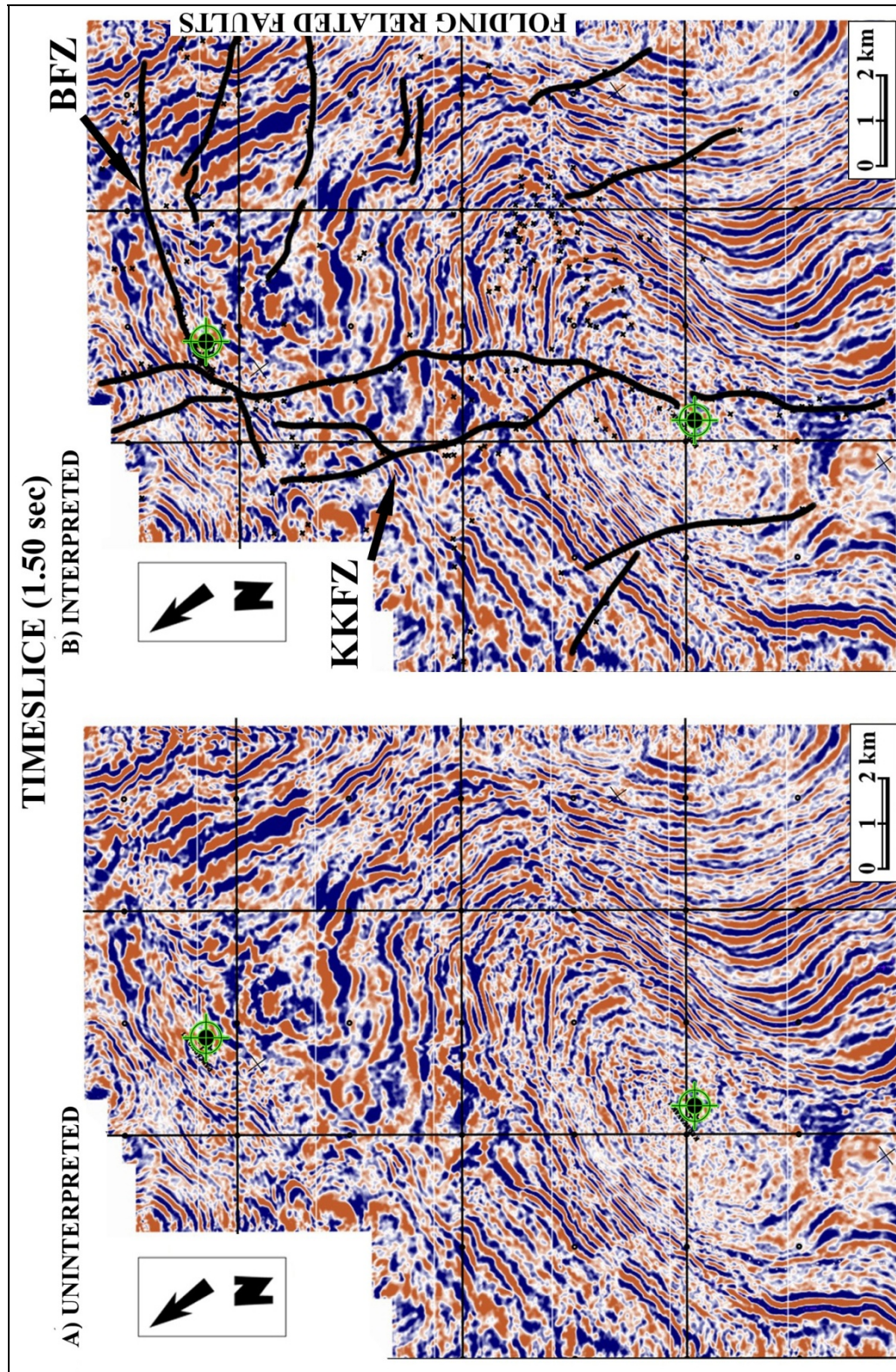


Figure 42: Raw (a) and interpreted (b) seismic time slices at 1.5 sec. BFZ: Babaeski Fault Zone, KKFZ: Karakavak Fault Zone.

The study area is characterized by two orthogonally oriented sets of faults that are trending NW-SE and NE –SW. Among these, Babaeski fault zone (BFZ) in the north reaching up to 11 km length consists of parallel strike-slip faults forming a positive flower structure that forms the Babaeski anticline. The NW-SE trending BFZ is part of the Trace fault system, which has been interpreted as the currently deactivated branch of North Anatolian Fault Zone (Perincek 1991, Coşkun 2000). The right-lateral strike-slip nature of the BFZ is clearly visible in time slices where right lateral offsets add up to approximately 1 km in the northeast section (Figure 40 and 41).

The other major fault zone trends in NE-SW direction extending beyond the survey area and is 18 km in length. This fault zone offsets the Karakavak fold and named as Karakavak fault zone (KFZ). The KFZ is characterized by several strike-slip splays branching out from the main strand in the north where it cuts and offsets the Babaeski Fault Zone near Babaeski town. This cross-cutting relationship is characterized with minor vertical offsets in seismic sections but displays noticeable left-lateral offsets in time slices. The amount of left-lateral offset on KFZ is measured from time slices using offset branches of BFZ as approximately 0.5 km (Figure 39 and 40).

In addition, there are also a number of short secondary faults across the Karakavak Anticline in the east. These faults are oriented in a radial pattern implying that faulting is mainly related to folding rather than strike-slip faulting (Figure 39, 40 and 41).

At the bottom, the recognized faults can be traced down to Eocene Ceylan group and occasionally down to the basement in the seismic sections (Figures 34-38). At the top, most of the faults cut the lower section of Mio-Pliocene Ergene group, but cannot be followed at shallower depths due to poor seismic data quality at shallower depths. At the surface, there is no evidence for the fault activity and Pliocene age Kırcaşalılı formation covers the entire region including faults interpreted from seismic data. Thus, the faults recognized in the study area, are inactive at least since Pliocene, which is supported by recent lack of seismicity in the region.

CHAPTER 5

DISCUSSION AND CONCLUSIONS

In this study, the deformation mechanism, fault kinematics and structural development of the central Thrace basin is revealed by using the 3D Temrez seismic data and available boreholes. The interpreted stratigraphic units include pre-Tertiary basement, Eocene Ceylan Group, Oligocene Mezardere, Osmancık and Danişmen formations and Mio-Pliocene Ergene Group. The study area is simply dominated by Miocene folds, two major strike-slip fault zones and secondary faults related to folding present in the region.

Throughout the study area, the Eocene and Oligocene basin fill is folded and overlain unconformably by unfolded Mio-Pliocene Ergene Group, which suggest that the recognized folds in the area, are developed synchronously during Miocene. Two major folds revealed in the study area are the Babaeski and Karakavak anticlines. The Babaeski Anticline which was recognized previously by Perinçek (1991) and Çoşkun (2000), is bounded by strike-slip fault segments forming a positive flower structure under transpression. On the other hand, the Karakavak Anticline which is recognized and mapped for the first time in this study, is not bounded by faults and much larger in size and seismic expression. In the study area, the both anticlines are characterized by a doubly plunging fold geometry and oriented approximately in E-W direction.

The Babaeski and Karakavak fault zones are the major fault zones recognized in the study area (Figure 43a). The Babaeski Fault Zone which is oriented approximately N65°W, is a right lateral strike-slip fault with significant reverse component. The Karakavak Fault Zone is a left lateral strike-slip fault

occasionally with minor normal component and displays two dominant trends which are in N15°E and N35°E directions. In addition to these fault zones, a number of secondary faults which are high angle to the fold limbs are developed in the region and they have multiple directions mainly dominated in N15°E and N65°W similar to the major fault zones.

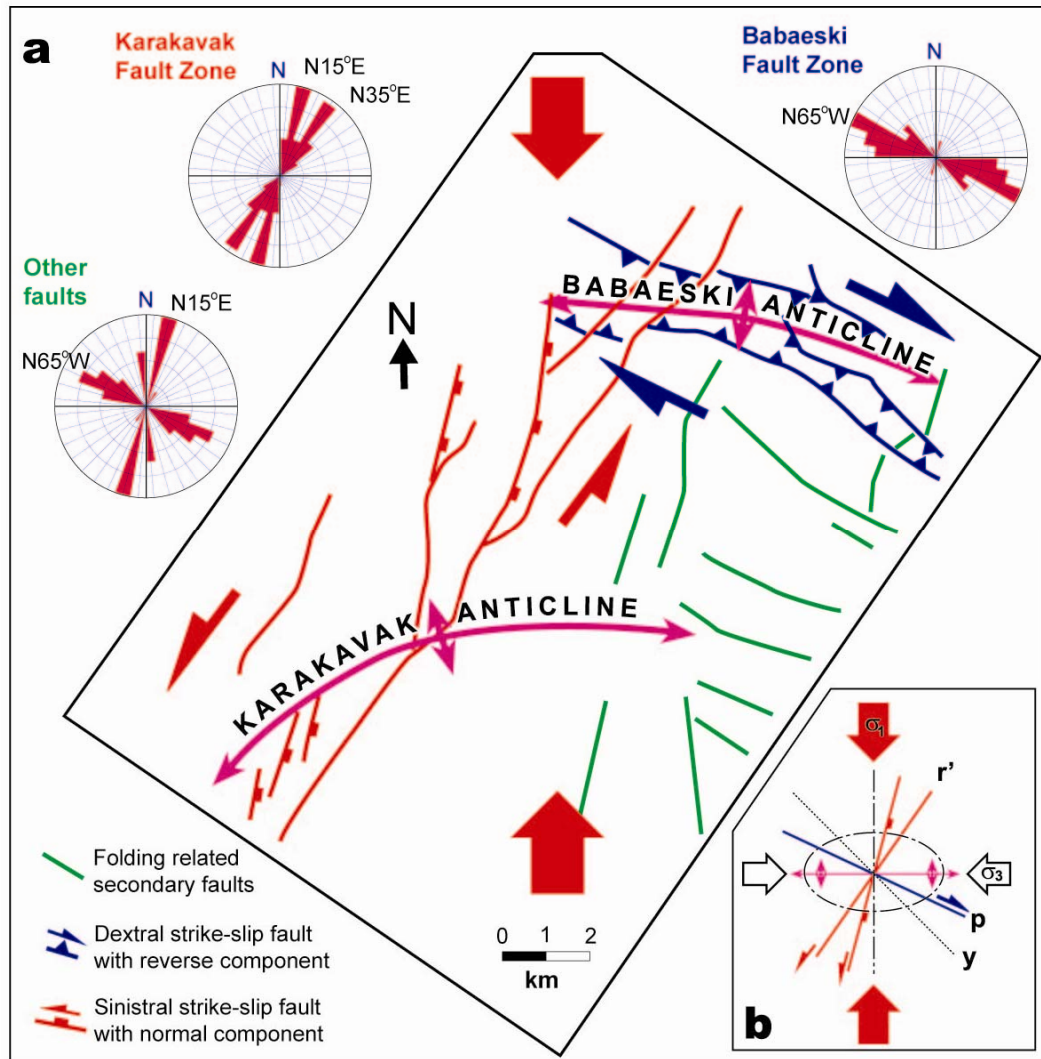


Figure 43: a) Major structures of the study area and their rose diagrams. **b)** Interpretation of the structures along the strain ellipse assuming that all the structures are developed under N-S (perpendicular to fold axes) regional compression and E-W extension.

In the study area, faults do not reach to the surface but cut through the Eocene-Oligocene basin fill up to the base of the Mio-Pliocene Ergene group. Thus, the active faulting initiated during Miocene synchronous to the folding under transpressional tectonic regime and ceased during Pliocene, which is in agreement with the previously proposed inception and deactivation ages of the Trace Fault System (Perinçek, 1991). In this respect, the deformation characterized by strike-slip faulting and folding in the study area, can be accounted as a precursor to the present day North Anatolian Fault Zone in the south.

The angle between the right-lateral Babaeski and the left-lateral Karakavak fault zones ranges between 80° and 100° . If these structures would have been formed contemporaneously under the same stress configuration, the observed geometric relationship can be replicated by using a strain ellipse constructed for a right-lateral sense of shear where the Babaeski Fault Zone aligns close to the main strand of the right-lateral fault system and Karakavak Fault Zone aligns with the left-lateral antithetic Riedel shear (Figure 43b). In this case, the orientation of major stress would be N-S, perpendicular to fold axes, and minor stress would be oriented E-W while intermediate stress is vertical. Such stress configuration would result in normal component along parts of the Karakavak Fault Zone while reverse component along the Babaeski Fault Zone as depicted in Figure 43.

In this scenario, the contemporaneous displacement and folding can be explained. However, present configuration of major stress based on earthquake moment tensor solutions is NW-SE. This implies that the structures in the study area became inactive either due to change in the stress configurations from N-S to NW-SE by Pliocene or due to approximately 30° clockwise rotation of the region as proposed by Kaymakci et al. (2007) based on paleomagnetic data. Since, there is no solid evidence for any change in regional stress direction in the past, the model that involves clockwise block rotation, is preferred in this study.

In the north, the splays branching out from the left-lateral Karakavak Fault Zone cuts and offsets the Babaeski Fault Zone. In an evolving strike-slip fault system, it is common to see such offsets that developed synchronously along a broad shear zone under the same stress configuration. Alternatively, the activity of the

Babaeski Fault Zone may have ceased earlier than the splays of the Karakavak Fault Zone during continuous clockwise rotation. At present, the age constraints and paleomagnetic data are not precise enough to make a distinction between these two possible scenarios.

Finally, the identified structures in this study such as folds, faults, unconformities etc. and their interpretations could be also beneficial for the petroleum industry since they have the potential to trap hydrocarbons.

REFERENCES

- Akartuna, M. (1953). Çatalca-Karacaköy bölgesinin Jeolojisi. *İstanbul University, Faculty of Science Monographies* , 13, 1-88.
- Atalık, E. (1992). Depositional system of the Osmancık Formation in the Tharce Basin. 366.
- Atalık, E. (1987). Trakya Havzası Soğucak Formasyonu çökel ortamları ve mikrofasiyes analizi. 92.
- Boer, N. P. (1954). Report on a geological reconnaissance in Turkish Thrace. *September, December G.A.* 25373.
- Bürkan, K. A. (1991). Trakya Havzasının organic jeokimyasal değerlendirmesi. *TPAO Company Report, no 2988* , 55.
- Coşkun, B. (2000). Influence of the Strandja-Rhodope Massifs and strands of the North Anatolian Fault on oil potential of the Thrace Basin, NW Turkey. *Journal of the Petroleum Science and Engineering* , 27, 1-25.
- Coşkun, B. (1997). Oil and gas fields-transfer zone relationships, Thrace Basin, NW Turkey. *Marine and Petroleum Geology* , 14, 401-416.
- Druitt, C. E. (1961). Report on the petroleum prospect of the Thrace-Turkey. *TPAO Company Report, no 1427* , 20.
- Ediger, V. Ş., & Batı, Z. (1987). Detailed stratigraphic, sedimentologic and palynologic investigation of the Hamitabat Formation from the Hamitabat-25 well. *TPAO Company Report, no 1185* , 1250.
- Elmas, A. (2003). Late Cenozoic tectonics and stratigraphy of the northwestern Anatolia: the effects of the North Anatolian Fault to the region. *Geologische Rundschau* , 92, 380-396.

Gerhard, J. E., & Alişan, C. (1987). Palynostratigraphy, paleoecology, and visual organic geochemistry of the Turgutbey-2, Değirmencik-3 and Pancarköy-1 wells, Tharce Basin, Turkey. 33.

Gökçen, N. (1971). Güneydoğu Trakya'nın Paleojen stratigrafisinde Ostracod'lar açısından yeni görüşler. *Proceedings of the First Petroleum Congress of Turkey* , 81-85.

Gökçen, N. (1973). Pınarhisar Formasyonu'nun yaşı ve ortam şartlarında görülen yanal değişimler (Kuzey, Kuzeydoğu Trakya). *Proceedings of the 50th Earth Sciences Congress* , 128-142.

Görür, N., & Okay, A. I. (1996). A fore-arc origin for the Thrace Basin, NW Turkey. 85, 662-668.

Holmes, A. W. (1961). A stratigraphic review of the Thrace . *TPAO Exploration Group Archive, Unpublished technical report, no 368* .

Hoşgörmez, H., & Yalçın, N. M. (2005). Gas-source correlation in Thrace Basin, Turkey. *Marine and Petroleum Geology* , 22, 901-916.

Huvaz, Ö., Sarıkaya, H., & Nohut, Ö. M. (2005). Nature of a regional dogleg pattern in maturity profiles from Thrace basin, northwestern Turkey: newly discovered unconformity or a thermal anomaly? *The American Association of Petroleum Geologists Bulletin* , 89, 1373-1396.

İslamoğlu, Y., Harzhauser, M., Gross, M., Jimenez-Moreno, G., Coric, S., Kroh, A. (2010). From Tethys to Eastern Paratethys: Oligocene depositional environments, paleoecology and paleobiogeography of the Thrace Basin, NW Turkey. *Geologische Rundschau* , 99, 183-200.

Kaymakçı, N., Aldanmaz, E., Langereis, C., Spell, T. L., Gürer, O. F., & Zanetti, K. A. (2007). Late Miocene transcurrent tectonics in NW Turkey: evidence from palaeomagnetism and ⁴⁰Ar-³⁹Ar dating of alkaline volcanic rocks. 144, 379-392.

Kemper, E. (1961). The Kırklareli limestone (Upper Eocene) of the northern basin . *General Directorate of Petroleum Affair Company Report* , 37.

Keskin, C. (1971). Pınarhisar alanının jeolojisi. *Turkish Geological Society Bulletin* , 14, 31-84.

Keskin, C. (1974). The stratigraphy of the northern Ergene basin-Thrace. *Proceedings of the second Petroleum Congress of Turkey* , 137-163.

Krausert, R., & Malal, Z. (1957). Measured cross-section of the Koyunbaba Member. *TPAO Exploration Group Archive, unpublished technical report #1433* , 1.

Lillie, R. J. (1999). *Whole earth geophysics: An introductory textbook for geologists and geophysicists*. Prentice Hall.

Okay, A. I., Özcan, E., Cavazza, W., Okay, N., & Less, G. (2010). Basement types, Lower Eocene Series, Upper Eocene Olistostromes and the Initiation of the Southern Thrace Basin, NW Turkey. *Turkish Journal of Earth Sciences* , 19, 1-25.

Özcan, E., Less, G., Okay, A. I., Baldi-Beke, M., Kollanyi, K., & Yılmaz, Ö. (2010). Stratigraphy and Larger Foraminifera of the Eocene Sallow-marine and Olistromal Units of the Southern Part of the Thrace Basin, NW Turkey. *Turkish Journal of Earth Sciences* , 19, 27-77.

Pamir, H. N., & Baykal, F. (1947). Istranca Masifinin Jeolojik Yapısı. *Turkish Geological Society Bulletin* , 1, 7-74.

Perinçek, D. (1991). Possible strand of the North Anatolian Fault into the Thrace Basin. *The Association of American Petroleum Geologist* , 75, 241-257.

Sakıncı, M., Yaltırak, C., & Oktay, F. Y. (1999). Palaeogeographical evolution of the Thrace Neogene Basin and the Tethys-Paratethys relations at northwestern Turkey. *153*, 17-40.

Schneider, W. A. (1978). Integral formulation for migration in two and three dimensions. *Geophysics* , 43, 49-76.

Şengör, A. M., & Yılmaz, Y. (1981). Tethyan evolution of Turkey: A plate tectonic approach. *75*, 181-241.

Şengör, A. M., Tüysüz, O., İmren, C., Sakıncı, M., Eyidoğan, H., Görür, N. (2004). The North Anatolian Fault: a new look. *33*, 1-75.

Siyako, M., & Huvaz, O. (2007). Eocene stratigraphic evolution of the Thrace Basin, Turkey. *Sedimentary Geology* , *198*, 75-91.

Sunal, G. (2008). Geological evolution of the Strandja Massif, Thrace Basin, Turkey. *Der Geowissenschaftlichen Fakultät, der Eberhard-Karls-Universität Tübingen, Ph. D. Thesis* , 158 .

Sünnetçioğlu, M. A. (2008). A sequence stratigraphic approach to the depositional history analysis of the upper eocene sedimentary succession, northwest of the Thrace Basin, Turkey. *METU, The Graduate School of Natural and Applied Sciences, Ph. D. Thesis* , 263.

Turgut, S. (1997). Depositional Sequences and Hydrocarbon Potential of the Tertiary Sediments of the Eastern Thrace Basin, Based on Sequence Stratigraphic Concepts. *METU, The Graduate School of Natural and Applied Sciences, Ph. D. Thesis* , 366.

Turgut, S., & Eseller, G. (2000). Sequence stratigraphy, tectonics and depositional history in eastern Thrace Basin, NW Turkey. *159*, 393-399.

Turgut, S., Turkaslan, M., & Perinçek, D. (1991). Evolution of the Thrace sedimentary basin and its hydrocarbon prospectivity. (ed. A. M. Spencer) *Generation, accumulation and production of Europe's hydrocarbons. Special Publication of the European Association of Petroleum Geoscientists* , *1*, 415-437.

Tüysüz, O., Barka, A., & Yiğitbaş, E. (1998). Geology of the Saros graben and its implications for the evolution of the North Anatolian fault in the Ganos-Saros region, northwestern Turkey. *Tectonophysics* , *239*, 105-126.

Ünal, O. T. (1967). Trakya jeolojisi ve petrol imkanları. *TPAO Exploration Group Archive, unpublished technical report, #391* , 80.

Yaltrak, C. (2002). Tectonic evolution of the Marmara Sea and its surroundings. *190*, 493-529.

Yaltırak, C., & Alpar, B. (2002). Kinematics and evolution of the northern branch of the North Anatolian Fault (Ganos Fault) between the Sea of Marmara and Gulf of Saros. *Marine Geology* , 190, 351-366.

Yaltırak, C., Alpar, B., & Hüseyin, Y. (1998). Tectonic elements controlling the evolution of the Gulf of Saros (northeastern Aegean Sea, Turkey). 300, 227-248.

Yılmaz, Y., Gökaşan, E., & Erbay, A. Y. (2010). Morphotectonic development of the Marmara Region. *Tectonophysics* , 488, 51-70.

Zattin, M., Okay, A. I., & Cavazza, W. (2005). Fission-track evidence for late Oligocene and mid-Miocene activity along the North Anatolian Fault in southwestern Thrace. 17, 95-101.